LUNDS UNIVERSITET

Spin-FET based on InGaAs/InP heterostructure

Master Thesis

Ricardo Moreira Sallse de Andrade

Supervisors: Prof. Hongqi Xu and Dr. Marcus Larsson

11/17/2011

Abstract

A new design based on the spinFET proposed by Datta-Das was fabricated, using a channel defined by etching on a 2DEG material and nanomagnets as top-gates. The magnetotransports properties were measured at low temperatures. Magnetoresistance changes with different behaviors were measured in different configurations and the presence of hysteresis showed the action of the nanomagntes. But, due to the device instabilities, no conclusion could be drawn since more detailed measurements were not possible. Also, due to the same instabilities, no spin precession manipulation could be carried.

Populärvetenskaplig sammanfattning

Genom nedskalning av mikroelektroniken, kan både prestanda, kostnad, och effektförbrukning förbättras och har därmed varit ett mål för elektronikindustrin. Dimensionerna är så låga i nuvarande teknik att parasitisk kapacitans och läckströmmar begränsar möjliga fördelar. Spintronik är en ny teknik under utveckling som skulle kunna erbjuda lösningar för dessa problem.

Spintronik är en gren av fysiken som använder elektronernas spin istället för deras laddning för att transportera, behandla och lagra information.

Elektronens spin, som är en kvantmekanisk magnetisk egenskap, har en klassisk motsvarighet i rörelsemängdsmomentet hos en roterande kropp. Om kroppen roterar i en riktning, kallas rörelsen för *spin-upp*, och om den roterar i motsatta riktningen kallas rörelsen för *spin-ned*. Genom att använda magnetfält går det att påverka elektronens spin eftersom elektronen beter sig olika under elektromagnetiska fält beroende på sin spin-riktning. Till exempel kan elektronens spin rotera och ändra sin riktning när elektronen rör sig genom ett elektriskt fält.

Känsligheten för en mätning av elektronens spin är mycket högre än för en mätning av dess laddning. Förutom detta, krävs det mindre energi och tid för att ändra elektronens spin än för att flytta på elektronen. Därmed borde det vara möjligt att tillverka en bättre ersättare till klassiska elektroniska komponenter. En sådan ersättare skulle kunna vara spin-fälteffekttransistorn (spin-FET).

En klassisk fälteffektransistor har en analogi i ventilen för en vattenledning. I vattenledningen finns det tryckskillnad mellan ledningens båda ändar (elektrisk spänningsskillnad mellan transistorns kontakter som kallas *source* och *drain*). Om ventilen är stängd (transistorn är strypt med en *gate*-spänningen i mitten på transistorkanalen), går inget vatten genom ledningen (ingen elektrisk ström genom transistorn). När ventilen öppnas aningen (*gate*-spänningen sänks aningen) börjar vatten flöda genom ledning (elektrisk ström börjar flöda genom transistorn). Om ventilen öppnas ytterligare (*gate*-spänningen sänks ytterligare) flödar ännu mer vatten genom ledningen (ännu högre elektrisk ström flödar genom transistorn).

I en spin-FET injiceras *spin-upp* elektroner in mot transistorn. På *drain*-sidan (ena kontakten) finns en barriär som släpper igenom endast *spin-upp* elektroner. Om ingen *gate*-spänning läggs på spin-FET-komponenten kommer elektronerna att hålla sin *spin-upp*-riktning och passera barriären. När en *gate*-spänning istället läggs på, kommer elektronens spin att rotera bort från *spin-upp*-riktningen och elektronen stoppas i barriären och ingen ström går igenom spin-FET-komponenten. I detta arbete tillverkades och karaktäriserades en sådan spin-FET-komponent med viss framgång.

Table of Contents

1 Introduction 5
2 Theory 8
2.1 Data-Das Spin-FET 8
2.1.1 Rashba effect 8
2.1.2 Spin-valve 10
2.2 New Spin-FET design 12
2.2.1 Rashba effect 12
2.2.2 Zeeman splitting 12
3 Fabrication 15
4 Measurement equipment 29
5 Magneto-transport measurements 33
6 Conclusions 44
7 Outlook 46
8 Acknowledgements 48
9 References. 49

1 Introduction

With the scaling of microelectronics, both performance, costs, power consumption can be improved and therefore this has been a goal from the electronic industry. This scaling has followed a famous law, Moore's law; in which states that roughly every two years, the density and performance of the integrated-circuit has to double [1]. It is known that planar electronics are getting to its limits, due to parasitic capacitances, and leakage currents [2]. Therefore new technologies are being developed to take the boundaries even further, like non-planar transistors[3], and Spintronics.

In the Spintronics, the spin of the electron is responsible for carrying the information instead of the more traditional charge of the electron [4]. Using this property, non-volatile memories based on the Giant Magneto Resistance (GMR) or the Tunneling Magneto Resistance (TMR) effect with a much higher information density than other technologies [5] could be constructed and are used on hard disks. To further take advantages of the spin property, another important device to be developed is the so called spin field-effect transistor (spinFET), which could switch from on to off state faster using less power.

The spinFET was a device proposed by Datta-Das [6] (Figure 1.1) where the current modulation is due to the spin-orbit coupling (SO) between the spin of the polarized current and the semiconductor material. Also, magnetic contacts would serve to inject spin polarized current and detect its orientation.

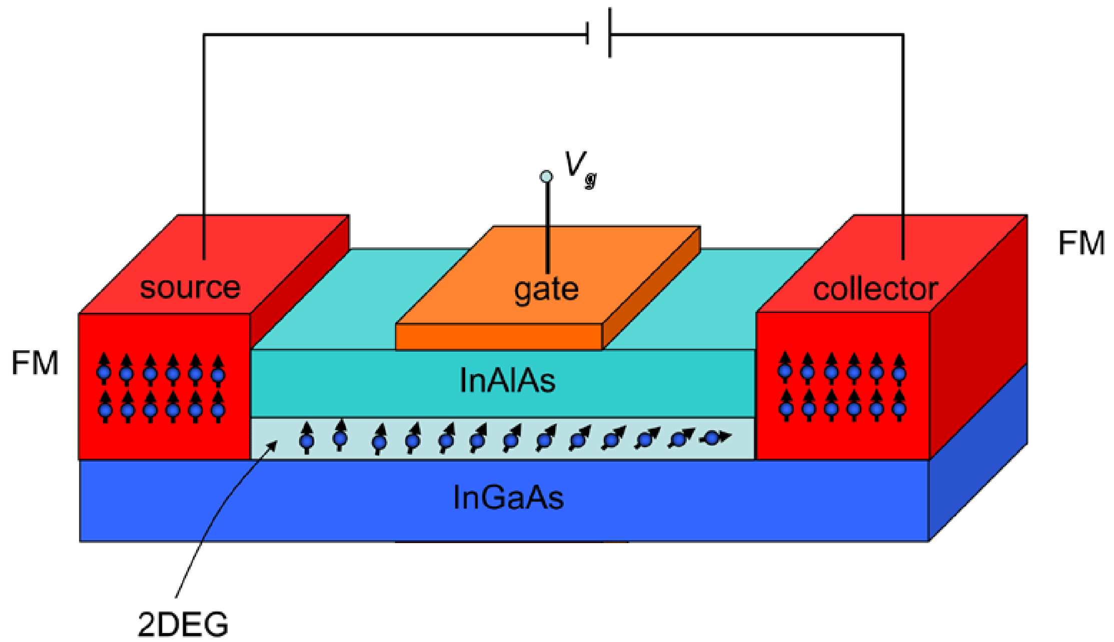

Figure 1.1 – Schematics of the Datta-Das spinFET. The ferromagnetic contacts (FM) are injecting and detecting spins that are polarized in the horizontal, pointing towards the right, while the arrows on the spheres represent the spin of the electron precessing due to the spin-orbit coupling. Extracted from [7]

In this work, a different design from the famous Datta-Das design was proposed. Instead of the spin injection through magnetic contacts, nanomagnets where placed on top of the semiconductor material to induce the spin polarization and side gates to act as the top gate in the original design, as shown in figure (1.2).

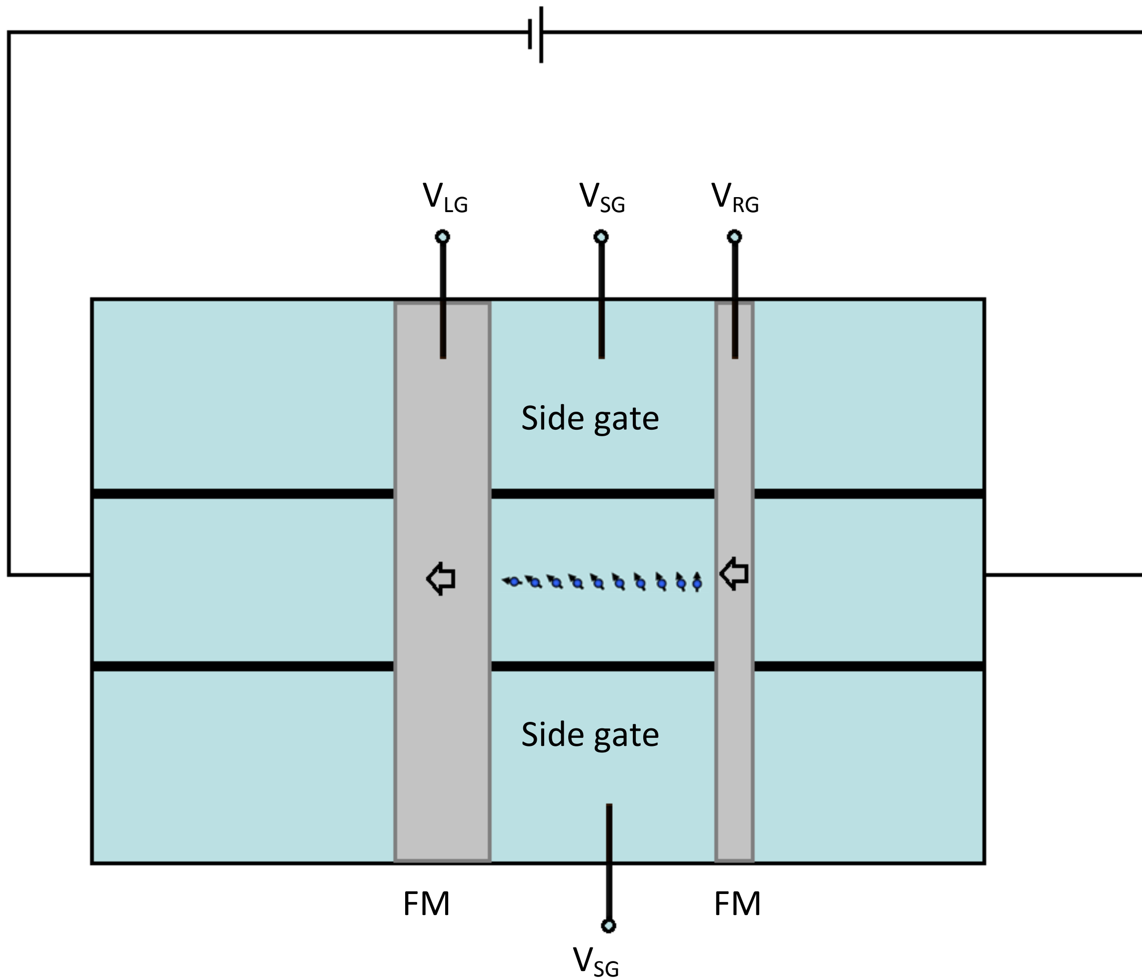

Figure 1.2 – Design proposed in this project. The bluish color represents a 2DEG material. A channel, where the current will flow, is defined by etching the material. The FM top-gates will serve as spin polarizers and detectors and the side gates will modulate the spin precession rate.

Although fabrication problems prevented all the components to work as expected, it was still possible to measure the effects of the magnetic field generated by the top-gates into the current flowing through the channel.

2 Theory

2.1 Data-Das Spin-FET

2.1.1 Rashba effect

Datta-Das proposed the spinFET device based on the Rashba effect. This effect can be described by the following Hamiltonian [8], also known as Rashba Hamiltonian:

$$H_{SO} = \alpha\vec{\sigma} \cdot \vec{k} \times \vec{\varepsilon} \qquad (2.1),$$

where α is the SO coupling, $\vec{\sigma}$ the Pauli matrices, $\vec{k}$ the electron momentum vector and $\vec{\varepsilon}$ the electric field.

The electric field from equation (2.1) appears in a 2D electron gas (EG) if its potential well is asymmetric, and this field is perpendicular to the plane where the 2DEG is formed.

Assuming that the 2DEG is formed in the *xy* plane (figure 2.1), the electron travelling along the *y* direction with $\vec{k}_y \neq 0$, $\vec{k}_x = 0$ and its spin is polarized along the *x* axis, the electrons with the *+x* polarization and with the *–x* polarization will have different energies, respectively [3]:

$$H_{SO} = \alpha\sigma_x k_y \varepsilon_z \qquad (2.2)$$

$$H_{SO} = -\alpha\sigma_x k_y \varepsilon_z \qquad (2.3),$$

even though there is no magnetic field applied. Therefore, this system acts as if in the referential point of the electron, the electron will feel the electric field as a magnetic field, since the electron is a charge moving in an

electric field. The magnetic field will be perpendicular both to the electric field and the electron momentum.

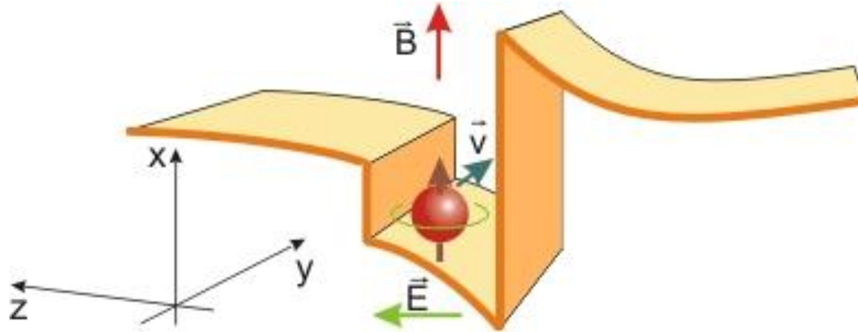

Figure 2.1 – Schematics of a 2DEG if asymmetric potential well. This asymmetry gives rise to the electric field in the *z* direction. For an electron travelling in the *y* direction, it will feel a magnetic field proportional to the electric field. This will produce a split in energy for electrons with different polarization, even if the external magnetic field is zero [9].

When combined with the effective mass Hamiltonian, the different polarizations will have the following energies:

$$E(\text{x pol.}) = \frac{\hbar^2 k_{y1}^2}{2m^*} - \alpha\sigma_x k_{y1}\varepsilon_z \qquad (2.4)$$

$$E(-\text{x pol.}) = \frac{\hbar^2 k_{y2}^2}{2m^*} + \alpha\sigma_x k_{y2}\varepsilon_z \qquad (2.5)$$

Equations (2.4) and (2.5) give:

$$k_{y1} - k_{y2} = \frac{2m^*}{\hbar^2}\alpha\sigma_x\varepsilon_z \qquad (2.6),$$

which means that a phase shift between the polarizations arises after a length *L* has been transversed:

$$\Delta\Theta = (k_{y1} - k_{y2})L = \frac{2m^*}{\hbar^2}\alpha\sigma_x\varepsilon_z L \qquad (2.7).$$

Analyzing the right side of equation (2.7), it can be seen that three components can change how much the polarized electron will precess, and which angle it will have. One is the SO coupling, α, intrinsic to the material and therefore cannot be manipulated; the electric field $\boldsymbol{\varepsilon_z}$, which is intrinsic to the heterostructure and the length *L*. Therefore, for a material with a defined *L*, an external electric field, $\boldsymbol{\varepsilon_{Ext}}$ can be applied parallel to the intrinsic one to increase

or decrease the precession rate. This can be achieved using a top gate as seen in figure 1.1, and equation (2.7) would then be:

$$\Delta\Theta = \left(k_{y1} - k_{y2}\right)L = \frac{2m^*}{\hbar^2}\alpha\sigma_x L(\varepsilon_z + \varepsilon_{Ext}) \qquad (2.8).$$

2.1.2 Spin-valve

To use the properties and consequences of the Rashba effect with an external electric field, it is necessary to inject a polarized current and then detect it. So a spin filter can be integrated to this system.

The injection of polarized current can be achieved using a ferromagnetic (FM) contact with a non-magnetic (N) conductor. Due to the spin dependent density of states (DOS) of a FM, which has a preferred spin population, if a potential is applied between this material and an N contact, spin polarized current will be injected in the later material (see figure 2.2). If another FM contact is connected to the device, this material will serve as a spin detector, decreasing the resistance when both FM have parallel magnetization and increasing when they have anti-parallel magnetization.

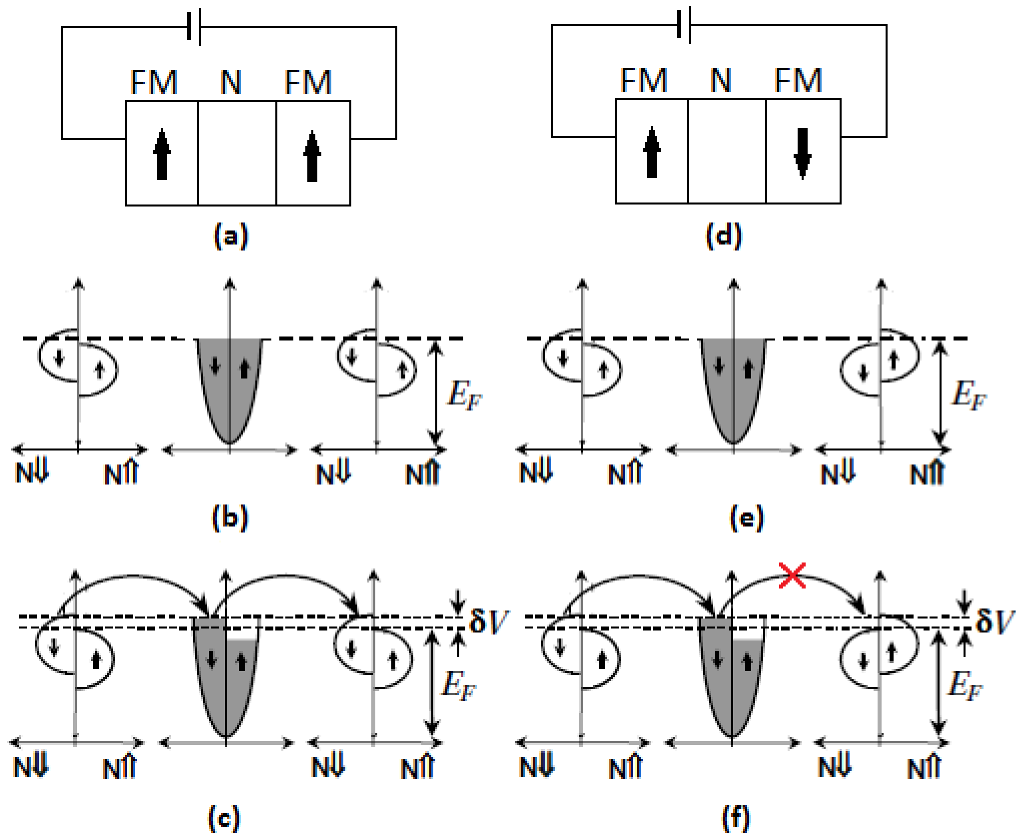

Figure 2.2 – Spin injection, spin accumulation and spin detection for the parallel (a), (b) and (c), and for the anti-parallel (d), (e) and (f), magnetization of the FM contacts. (a) and (b): schematics of the spin-valve device. At equilibrium, (b) and (e), it can be seen that the N material has an even distribution of spins on its DOS. On (b), both FM materials favor the spin-up state, lowering its energy. On (e), the left FM favors the spin-up state, while the right one favors the spin-down. If a potential is applied between the contacts, (c) and (f), it can be seen that the spin-down will be injected from the left FM onto the N material, where it will accumulate. When the magnetization is parallel (c), the spin can then go from the N material to the FM, since it has energy and the right configuration to fill a state; on the other hand, when the magnetization is anti-parallel (f), there is not free states for the spin to go to the FM material, therefore, there is no current. Modified from [10].

Combining the spin filter, with a semiconductor channel made with an asymmetric heterostructure, the spin modulation using a gate can theoretically be accomplished.

Work has been done on both fronts to achieve spin modulation on a 2DEG and to inject spins into a semiconductor material. Although the former was shown by measuring the Shubnikov-de Haas oscillations [11], the latter proved to also be possible but at very low efficiency, with effects within noise levels [12], possibly due to the resistance mismatch between the FM and the semiconductor material [13].

2.2 New Spin-FET design

As a possible solution, a different design from the Data-Das one is proposed, figure 1.2, although still based on it. There are basically two differences, one in the way on which the spin modulation is conducted, and the process of injecting and detecting the spin. These changes are motivated by the low spin injection efficiency on a semiconductor material, and the simplification of the fabrication.

2.2.1 Rashba effect

Taking again the Rashba Hamiltonian:

$$H_{SO} = \alpha\vec{\sigma}\cdot\vec{k}\times\vec{\varepsilon} \quad (2.1),$$

Instead of changing the effective value of the electric field $\boldsymbol{\varepsilon_z}$ (see figure 1.1), the electric field applied is parallel to the *xy* plane, therefore changing the momentum of the electron, ***k***. The difference in precession can be seen using the middle part of equation (2.7):

$$\Delta\Theta = \left(k_{y1} - k_{y2}\right)L = \frac{2m^*}{\hbar^2}\alpha\sigma_x\varepsilon_z L \quad (2.7).$$

Having all other terms constant, one can increase or decrease the precession rate of the spin by tuning the ***k*** vector.

2.2.2 Zeeman splitting

Since the efficiency is low when a spin is injected from a FM material to a semiconductor one, the solution tried in this work was to use a nanomagnet on top of the 2DEG material. The fringe field produced by this nanomagnet could induce a Zeeman splitting in the channel, therefore lowering and increasing the energy of parallel and anti-parallel spins. On an ideal case (figure 2.3), when a DDP is applied, only electrons with up spin will have enough energy to be in the region bellow the nanomagnet. The next region has no influence on an external magnetic field, allowing any spin to go through, but

since only certain spins could pass the previous region, it is expected that a polarized current will flow. Once this current reaches the region with the second nanomagnet, there are two possibilities. If the nanomagnet is magnetized parallel to the first one, then it will split the band, allowing these electrons to go through it and a current can be measured. If the nanomagnet has an anti-parallel magnetization, then the splitting will be inversed, having the down spin configuration with lower energy. Therefore, the polarized electrons won't have energy to go through and no current can be measured.

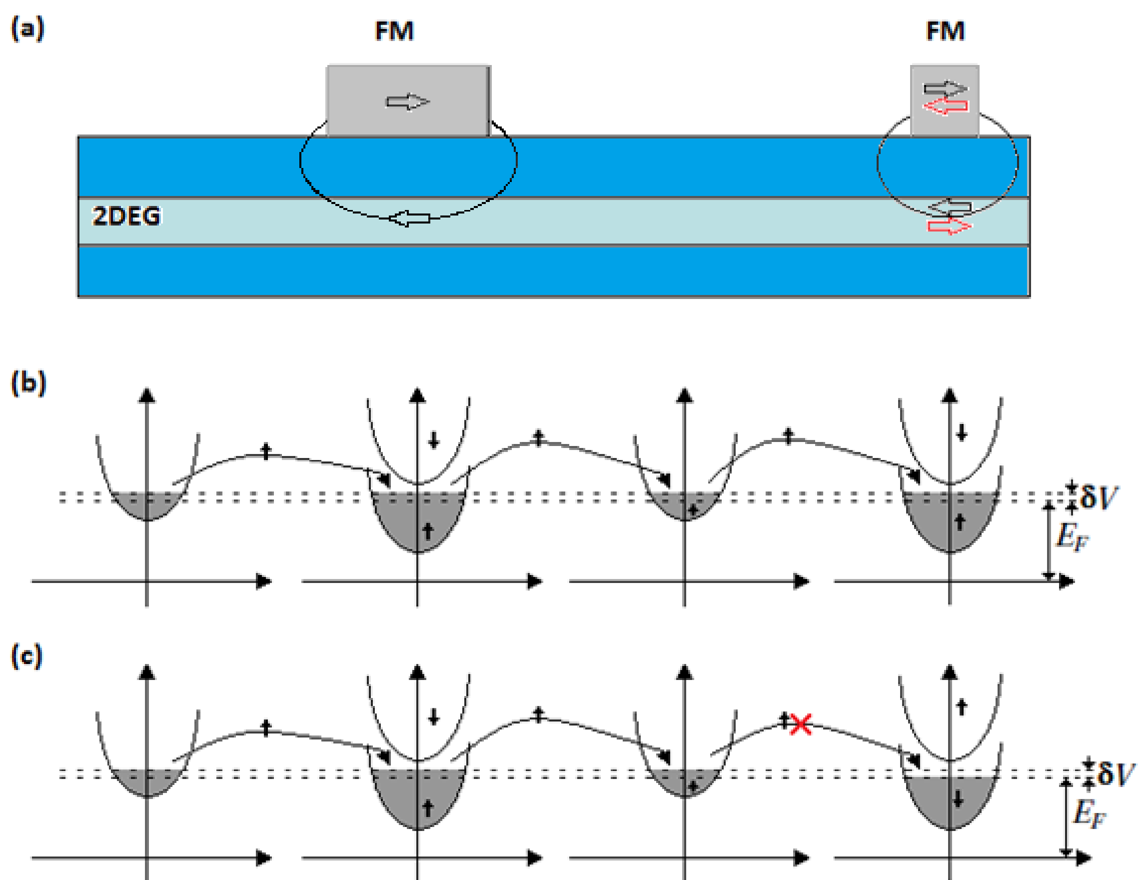

Figure 2.3 – a) Device schematics showing FM magnetization and the induced magnetic field around the 2DEG. b) DOS in the different regions of the 2DEG for the parallel-magnetized case (black arrows on the right), and c) for the anti-parallel magnetization (red arrows on the right). As it can be seen, the magnetic field from the nanomagnets induces a Zeeman splitting in the band, favoring one type of spin, therefore allowing only one kind of spin to go through, emulating the functionality of a spin-valve described previously.

Since the saturation magnetization of the FM depends on its geometrical size, the two nanomagnets were made so one would be twice as large as the other. By forcing these different characteristics in each nanomagnet, it is possible to switch their magnetization using an external magnetic field either to the parallel or the anti-parallel configuration compared to each other.

3 Fabrication

The fabrication process started with an InP/InGaAs heterostructure as shown in figure 3.1. This heterostructure is formed by an InP substrate, a 50nm thick InP buffer layer, a 9nm $In_{0.75}Ga_{0.25}As$ layer, where the 2DEG is formed, a 20nm InP spacer, a 1nm Si doped InP, to increase carriers mobility, and a 20nm InP cap layer.

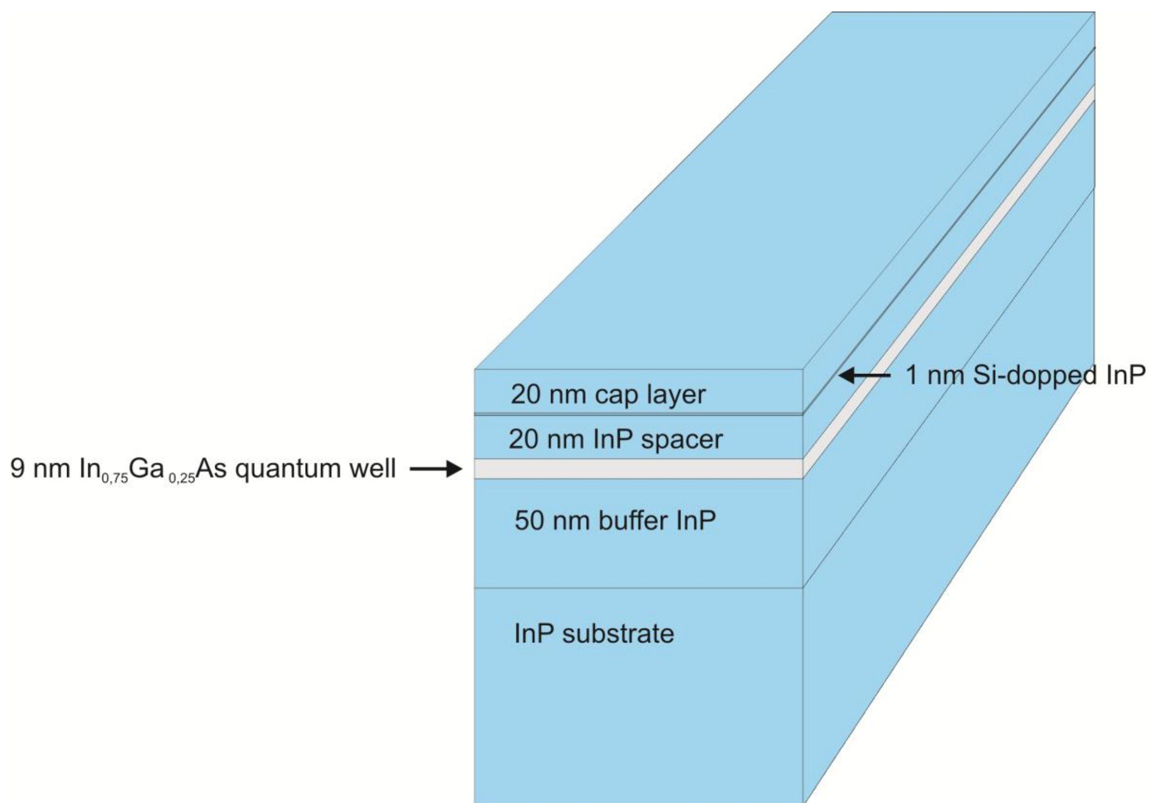

Figure 3.1– InP/InGaAs heterostructure. The quantum well is formed at the InGaAs layer, between the 20nm InP spacer and the 50nm InP buffer layer. The Si doped layer is used to increase carrier mobility.

The first step was to define the mesa that will contain the structure and the contacts to the measuring equipment (Figure 3.2).

A layer of ZEP520 A7 [1] resist was spun on the substrate at 6000 RPM for 45 seconds and then it was placed for a soft bake for 15 minutes at 160°C on a hot plate. This procedure was repeated once more to achieve a thicker layer, since this step does not require a good resolution.

The substrate was then exposed using a Raith150 Electron Beam Lithography system. Table 3.2 comprises the information of parameters for all EBL steps.

The substrate was then developed with o-Xylene for 5 minutes and etched with a freshly prepared mixture of 5 ml of HBr, 5 ml of HNO_3, 300 μl of saturated bromic water (SBW) and 40 ml of DI water for 2 minutes. The resist was then removed by dipping the substrate in Remover 1165 for a few minutes.

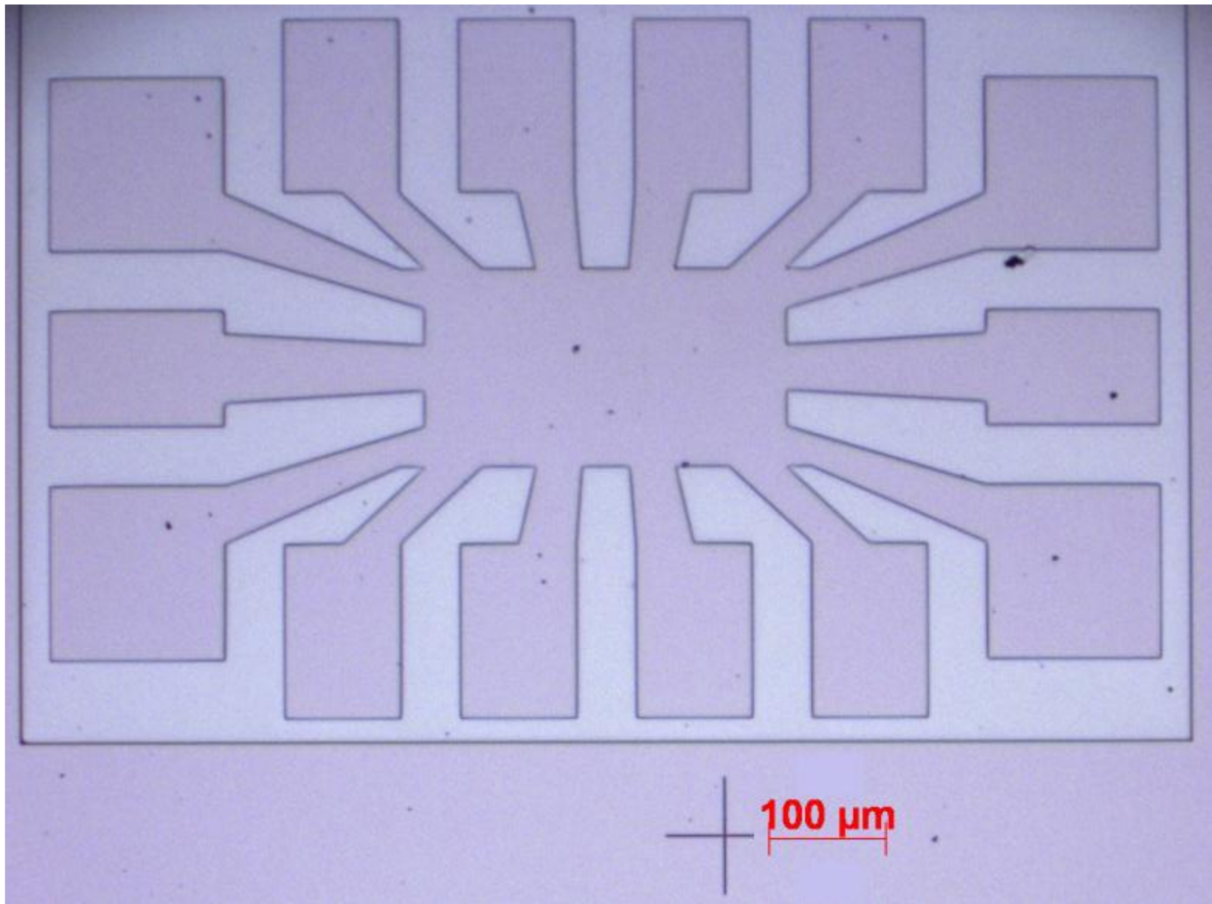

Figure 3.2 – Mesa. Optical image of the substrate after the MESA region was defined by etching. The lighter color represents the area that was etched away.

To evaporate the ohmic contacts (Figure 3.3), a layer of PMMA A6 was spun at 6000 RPM onto the substrate, followed by a soft bake for 15 minutes at 160°C. The substrate was then exposed by the EBL system and developed for 60 seconds with MIBK/IPA mixture. After placing it in an evaporator, model AVAC, it was evaporated 400Å Au/200Å Ge/1600Å Au. The substrate was placed for a few hours in acetone and a few seconds in ultrasonic bath to perform the lift-off. When the lift-off was finished, the sample was placed on a rapid thermal process (RTP) equipment, a UniTemp RTP-1200, to anneal the contacts. The temperature was raised from room temperature to 390°C in 120 seconds, and kept at this level for 80 seconds.

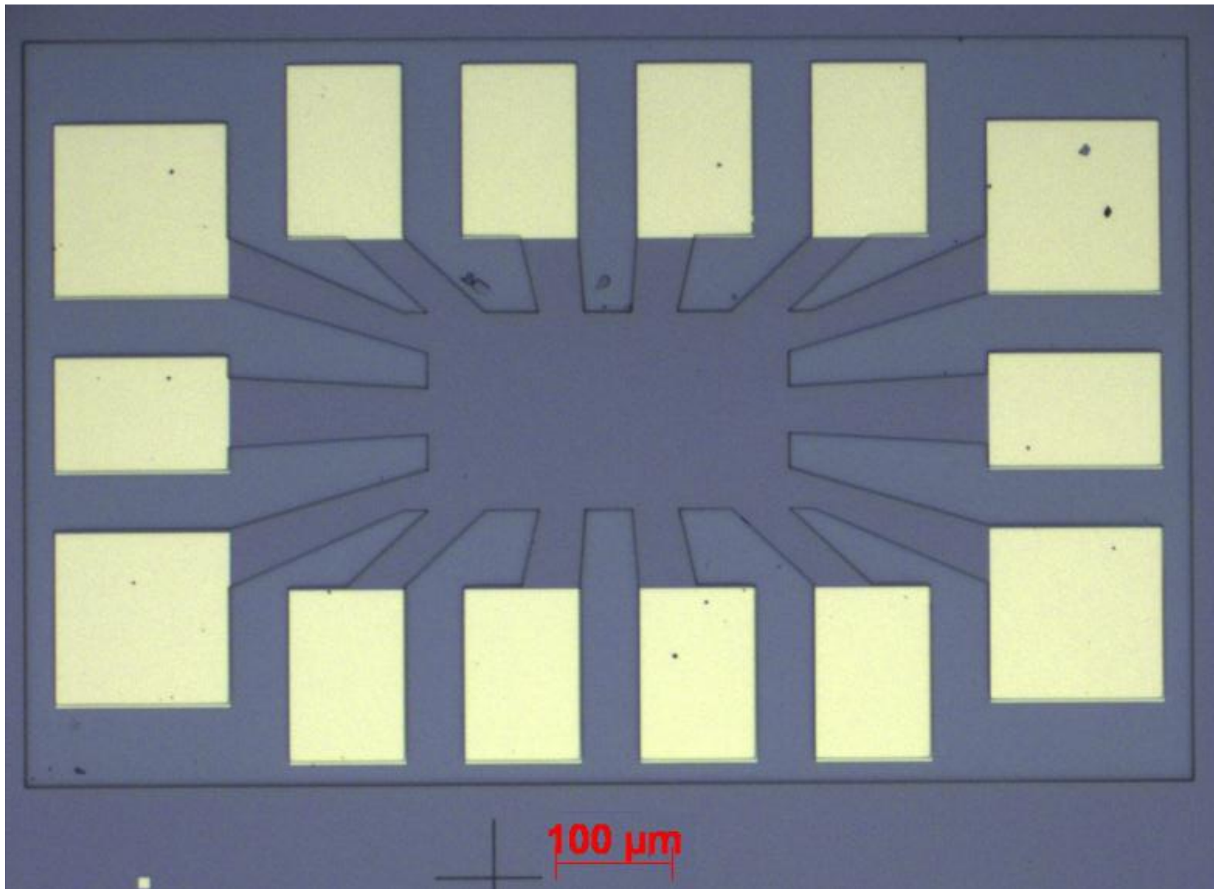

Figure 3.3 – Optical image of the MESA, where the yellow regions are the contacts after lift-off and annealing.

The next step was done to define the channel and isolate some of the contacts by etching (Figure 3.4).

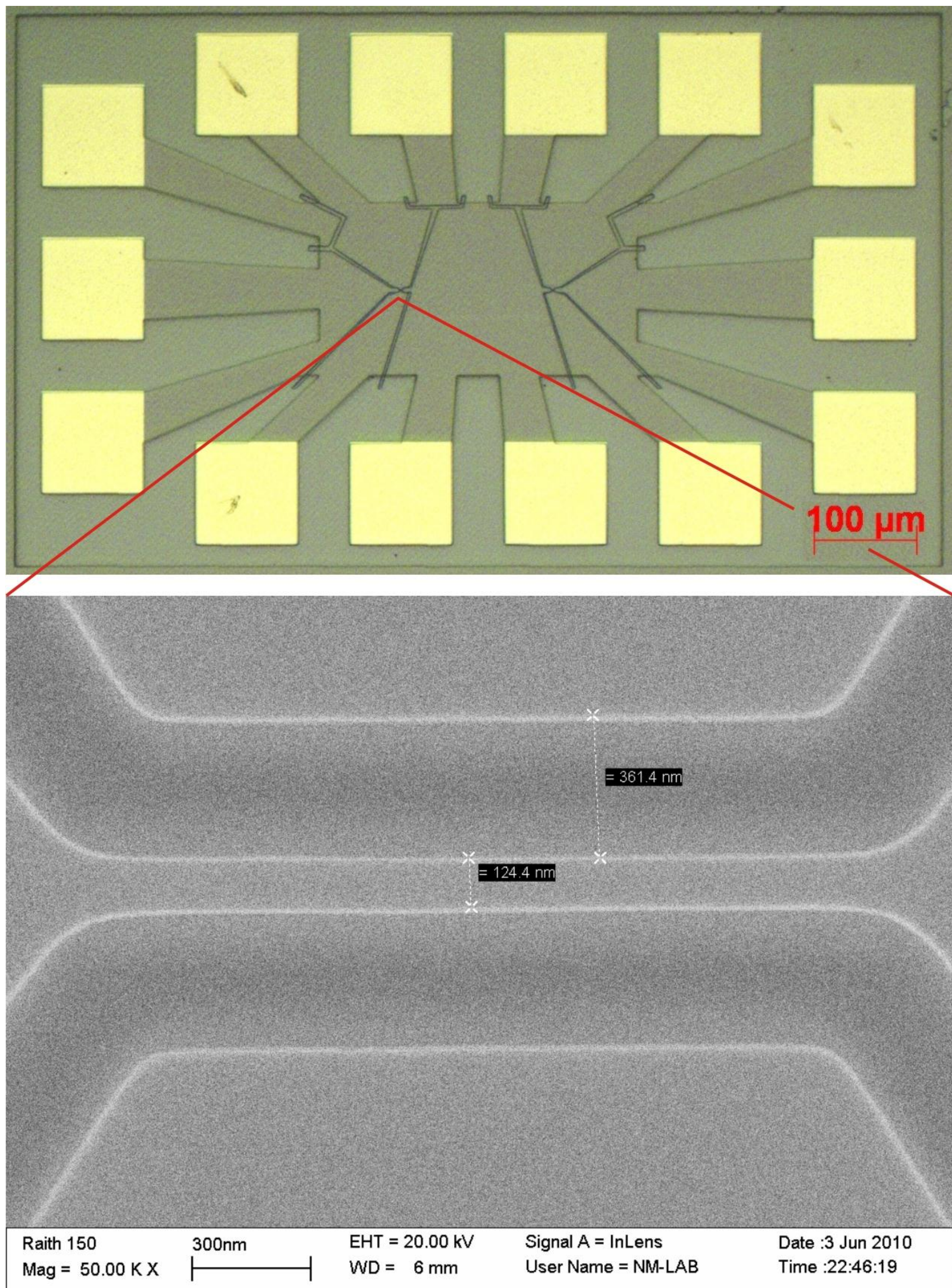

Figure 3.4 – Top) Optical image of the fine etch and contacts isolation. Bottom) SEM image of the 124 nm thick channel. The etched region is approximately 360nm wide and is represented as black lines on the optical image.

A single layer of ZEP520 A7 was spun onto the substrate for 60 seconds at 9000 RPM. A 10 minutes soft bake at 160°C was performed in a closed environment. The resist was exposed in the EBL system and developed with o-Xylene for 5 minutes. It was then post baked for 2 minutes at 120°C on a hot plate with closed environment.

A fresh mixture of 3ml of HBr, 3ml of HNO_3, 300 μl of SBW and 60ml of DI water was used to etch the substrate for 20 seconds.

The channel sizes were designed to be in between 80 and 140 nm, because it was desired that the channel should have very few conductance channels.

To isolate the substrate from the top-gates, a dielectric layer was deposited by atomic layer deposition (ADL) technique (Figure 3.5). It was chosen to be HfO_2 because it has a high dielectric constant so only a thin film is necessary to isolate the channel.

Table 3.1 – ALD parameters

Step	Instruction	Value
1	N_2 flow	20sccm
2	precursor temperature	75°C
3	chamber temperature	100°C
4	TDMA Hf pulse	0,1 seconds
5	wait	80 seconds
6	Water pulse	0,025 seconds
7	wait	80 seconds
8	go to step 4	160 times

To define the area where the dielectric would be deposited, the same exposure procedure used for the contacts was used here. After the development, the substrate was placed on an ALD system Savannah 100, where a 15nm HfO_2 was deposited at low temperature (Table 1) to increase

film quality. This deposition takes several hours due to the low temperature, where time has to be given so the atoms will spread throughout the surface and reach the lowest energy level configuration. The lift-off procedure from the contacts was used once again.

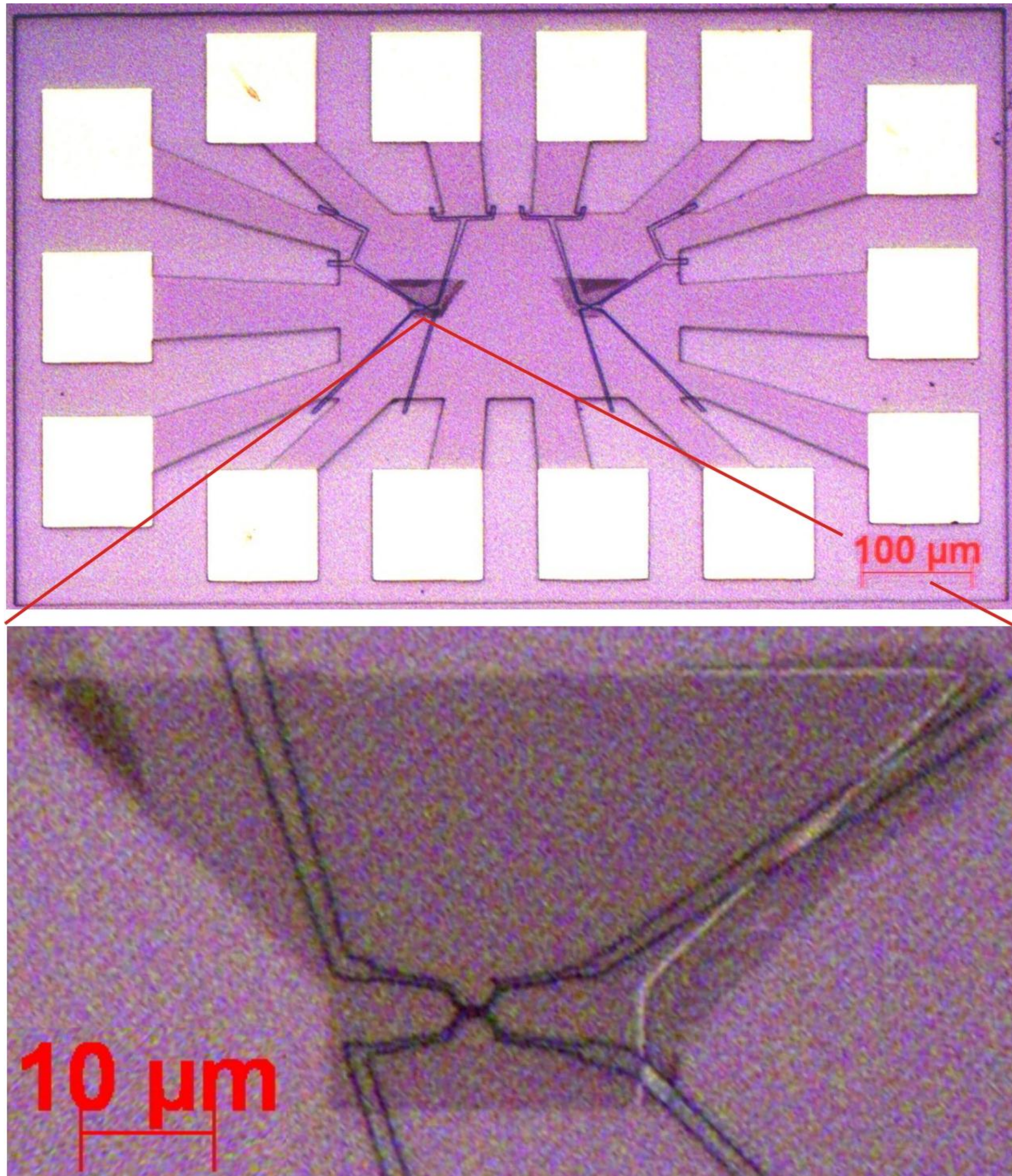

Figure 3.5 – Top) Optical image of the MESA. The trapezoidal region on top of the channel is the HfO_2. Bottom) Zoom in on the channel region.

To isolate the leg between the contacts and the top gates, a layer of cross-linked resist was deposited (Figure 3.6).

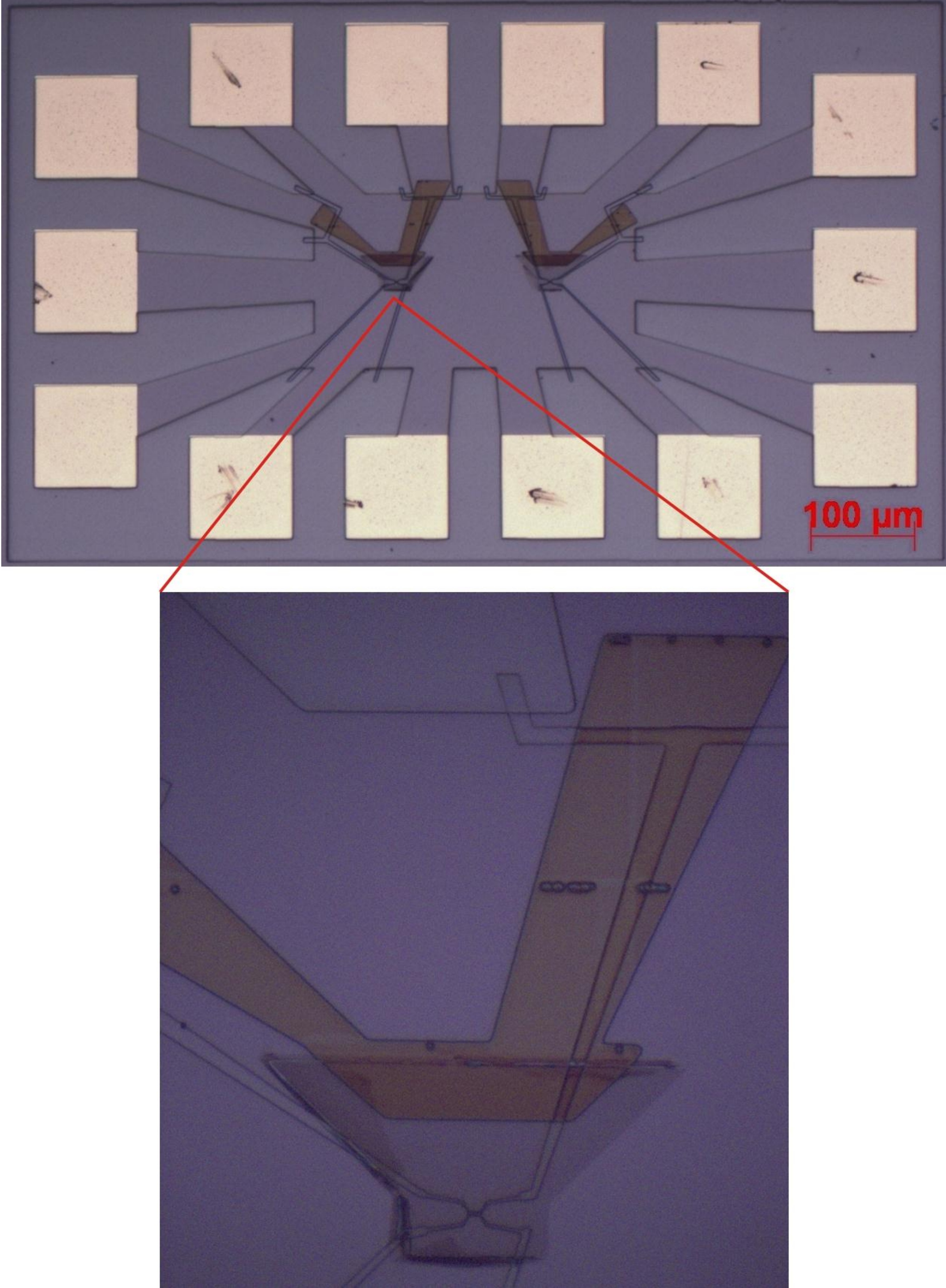

Figure 3.6 – Top) Optical image of the PMMA isolation for the leg between the contacts and the top gates (darker color). Bottom) Zoom in showing the PMMA overlapping with the HfO_2 film.

A layer of PMMA 950A6 was spun on the substrate for 30 seconds at 6000RPM and soft baked in the hot plate for 10 minutes at 160°C. The resist was cross-linked with a high dosage EBL and developed for 2 minutes in acetone. A post development bake of 15 minutes at 180°C was performed.

The last fabrication step was the evaporation of the top gates (Figure 3.7). Since it was used a Ferromagnetic material, this step was performed a few hours before the substrate was loaded into the Cryostat to decrease the time it was exposed to air, minimizing oxidation. The ferromagnetic material chosen was a Fe/Co alloy, which has a magnetic moment of approximately 2,3μ_B, higher than pure Co, which has around 1,6 μ_B [14], so the magnetic field could be higher at the 2DEG, and each gate had a different size, so its magnetization would switch at different external magnetic field.

A layer of PMMA 200A5 was spun for 30 seconds at 6000RPM onto the substrate and it was soft baked on a hot plate for 10 minutes at 160°C. It was then exposed using the EBL and developed in MIBK/IPA for 90 seconds. The substrate was then placed in a PlasmaPreen system, using a faraday cage around it, to remove any resist residues. The sample was then placed in the Evaporator to evaporate 75Å Ti/750Å CoFe alloy.

The lift-off was done by dipping the sample for a few hours into a refrigerated acetone (~3°C) for a few hours to slow down the resist dissolving process.

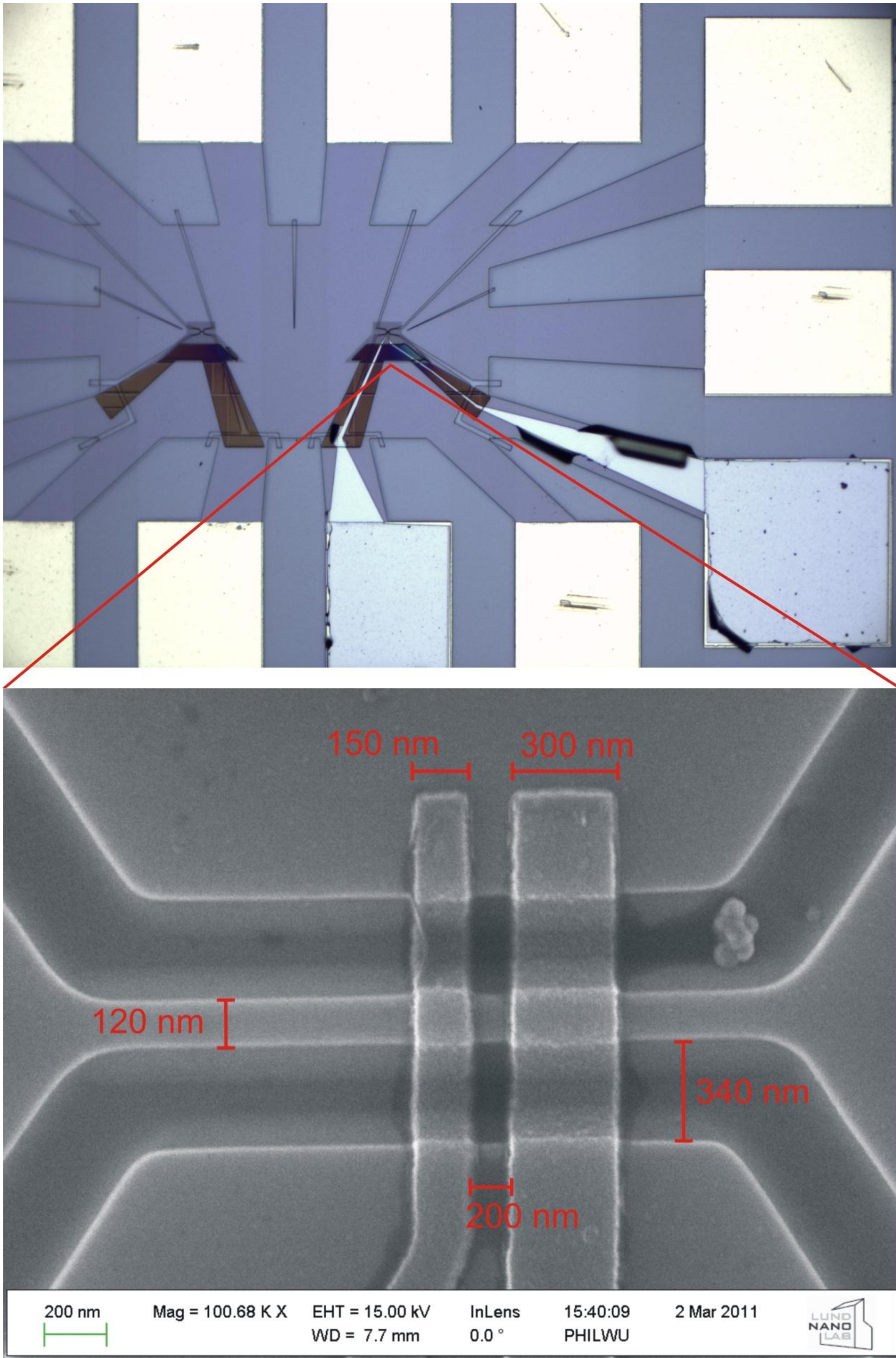

Figure 3.7 – Schematic of the top gates and the contact legs in light grey (top). SEM image of the etched channel with the deposited top-gates (bottom).

This step was later added after a few samples had presented a delamination of the metal gates. It was thought that due to poor adhesion of the alloy even with the Ti sticking layer, combined with the very fast lift-off process would create enough stress on the thin gate to break it (figure 3.8).

Although through optical images this problem seemed to be solved, some electric characterization of the gates still shows problems with this step (figure 3.9).

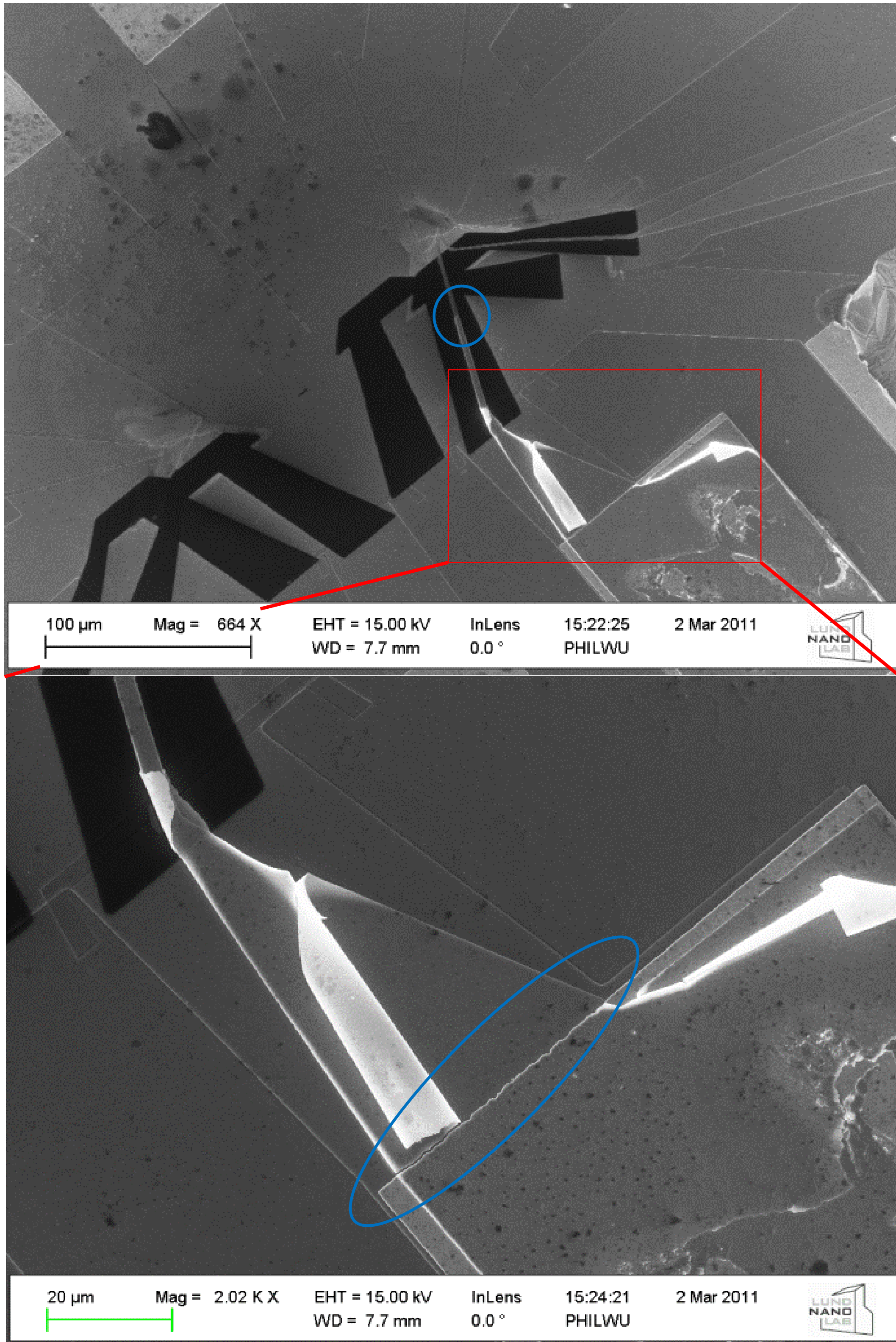

Figure 3.8 – Top) SEM image after top-gate lift-off and electrical measurements in the cryostat. It can be seen in the left image that color of the gate-legs change (blue circle), probably due to the peel-off of the alloy. The red square is zoomed (bottom image), and it is clear that the alloy is peeling-off and that there is a crack (blue circle), most likely losing the electrical connection.

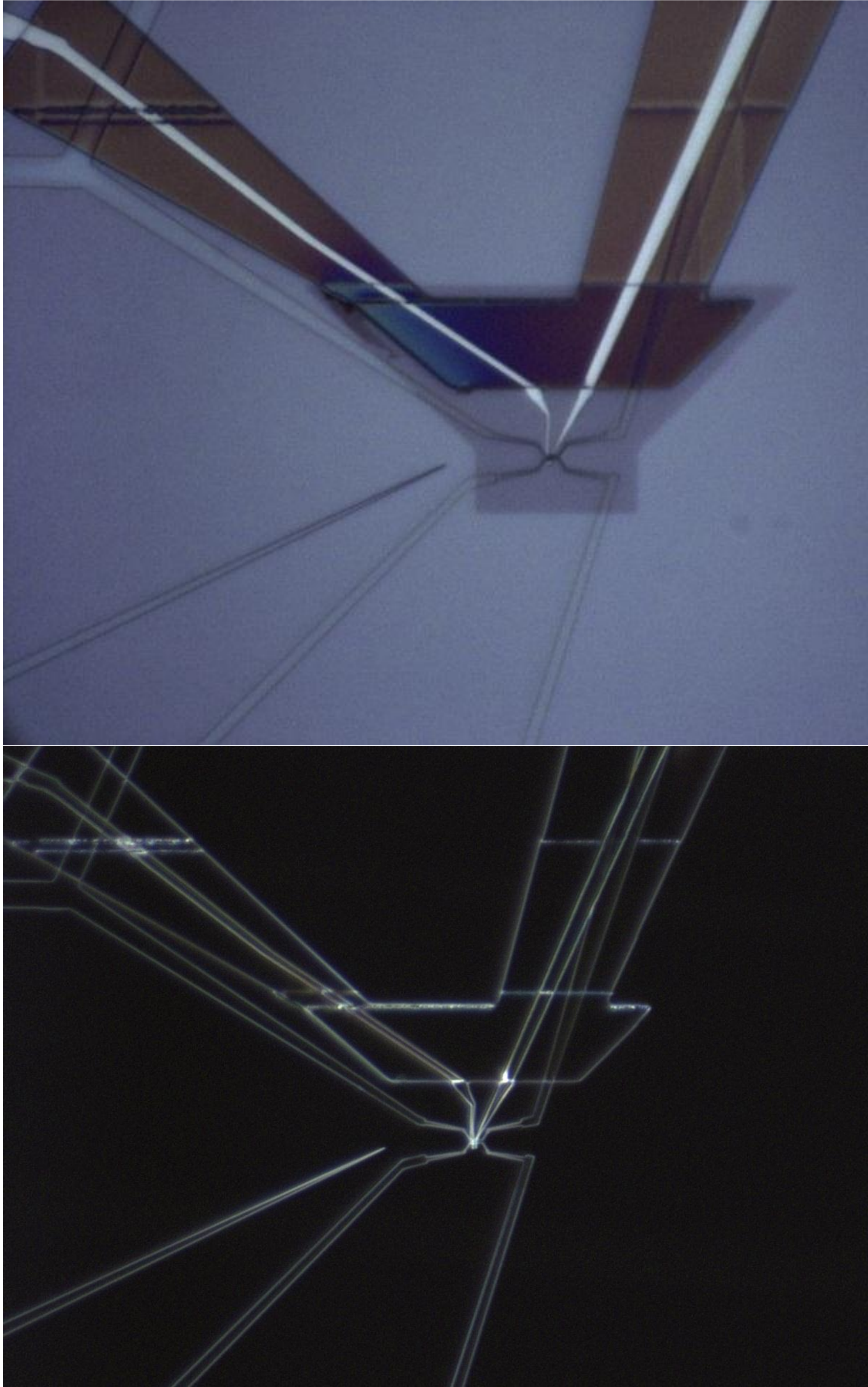

Figure 3.9 – Left) Bright field optical image. There is no apparent defects on the top gates. Right) Dark field optical image. It can only be seen the interface between the materials, showing again that the top gates are in good condition.

The substrate is finally mounted on a plastic chip carrier with 14 contacts, and its contacts were bonded in a KS 4523 digital bond-machine to its metal legs. This plastic chip carrier is connected to the tip of the cryostat stick. The stick is then lowered into the dewar and the electrical connections are made for the measurements.

Tabel 3.2 – Exposure parameters for the EBL steps.

Step	Mesa	Contacts	Fine etch	HfO_2	Cross-linked PMMA	Top Gate
Resist	ZEP 520A7	PMMA 950A6	ZEP 520A7	PMMA 950A6	PMMA 950A6	PMMA 200A5
Acceleration voltage (kV)	20	20	20	20	20	20
Beam aperture (um)	120	120	7.5	120	120	7.5
Area dose ($\mu C/cm^2$)	30	210	30	210	20000	210
Line dose (pC/cm)	Non applicable (n/a)	n/a	150	n/a	n/a	n/a

4 Measurement equipment

The measurements were carried out in a ^{4}He Cryostat (Figure 4.1) from Janis Research Co. with temperatures varying from 1.5 to 1.7K.

The cryostat also has a toroidal superconductor magnet with its symmetry axes along the symmetry axes of its dewar.

The electric equipment used for the measurements were:

- Stanford lock-in amplifier model SR830;
- Stanford low-noise current pre amplifier model SR570;
- Hewlett-Packard multimeter model 34401A;
- Low-frequency pass filters;
- Current divider;

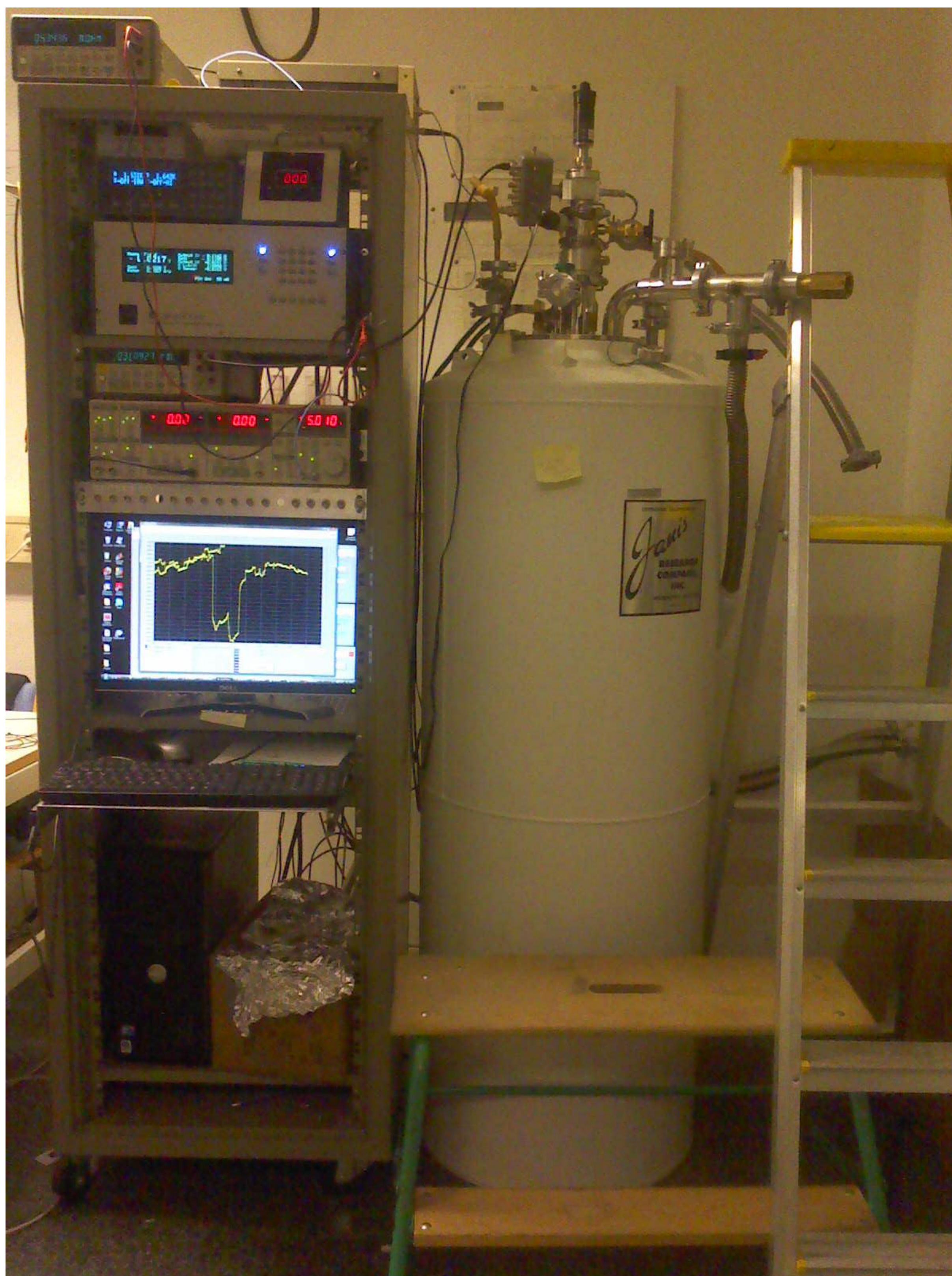

Figure 4.1 – Cryostat dewar (middle) and inserts.

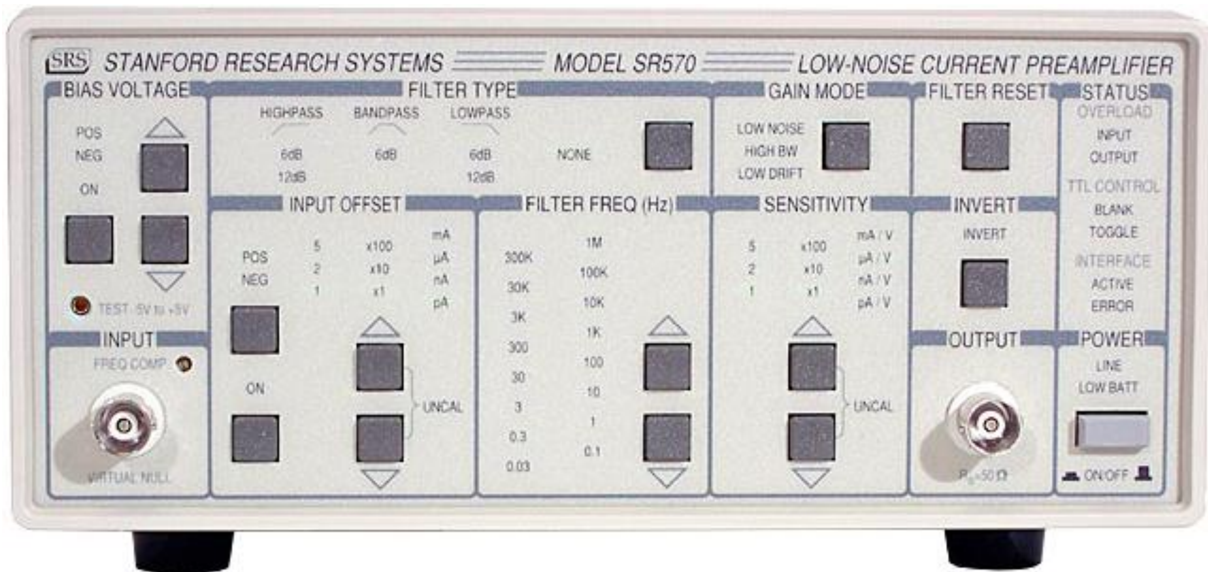

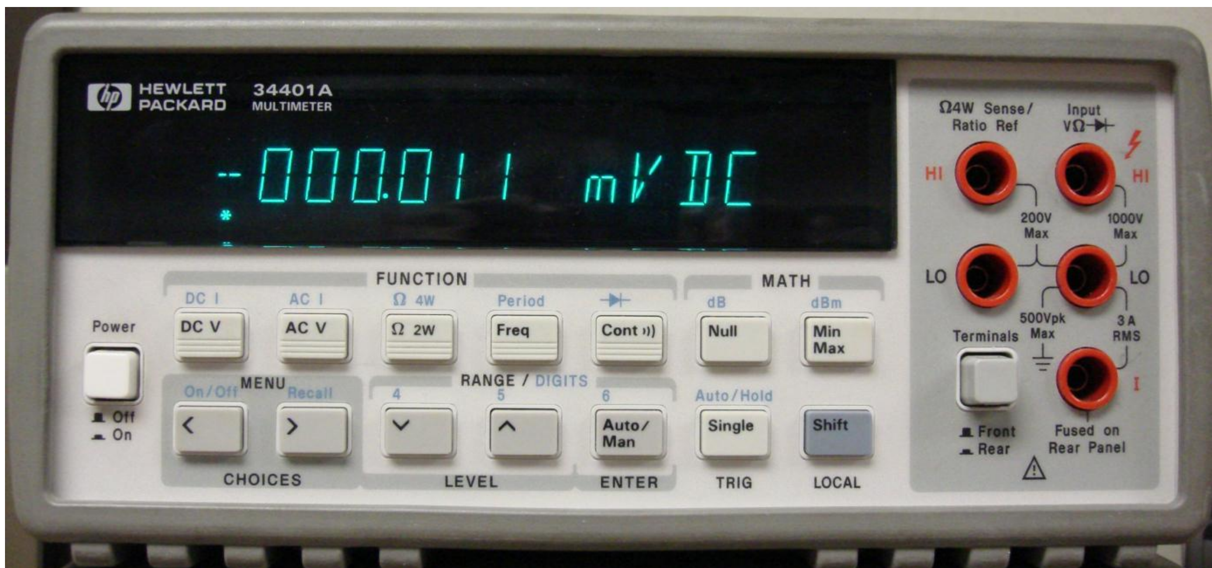

Figure 4.2 – From top to botton: Lock-in amplifier; pre-amplifier; multimeter.

The circuit schematic for measuring the device is the following:

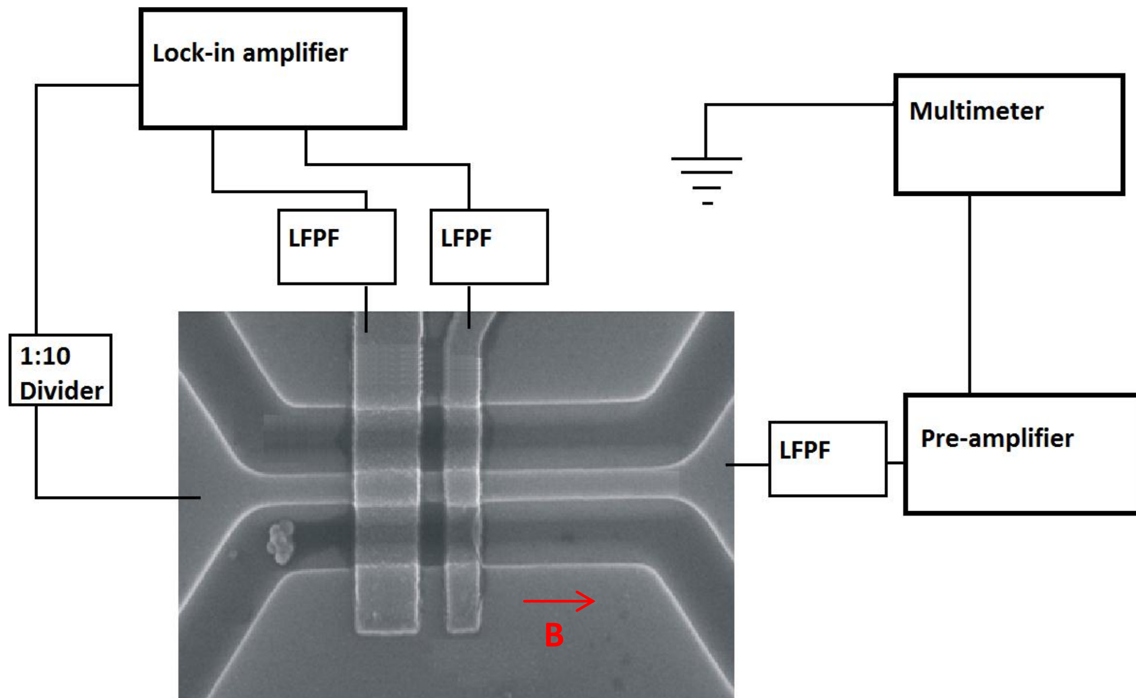

Figure 4.3 – The voltage is applied in the channel source contact using the lock-in amplifier and going through a 1:100 divider. The lock-in is also responsible for applying a DDP on the top gates. The pre-amplifier is connected to the channel drain and it is connected to the multimeter. All lines have a low-frequency pass filter (LFPF) to minimize the noise.

5 Magneto-transport measurements

The first measurements made on the device were leakage measurements between both the top gates and the channel, both side gates and the channel, both side gates and the top gates and between the top gates. To perform this, a simple IxV curve was measured between the two desired terminals. All measurements showed no leakage, with the exception of the side gates and the channel. Therefore, from the beginning, these gates could not be used, and the change in the precession rate of the spins of the electron given by equation (2.7) could not be checked.

It was then applied a voltage along the channel and it was measured the current versus the top-gate voltage.

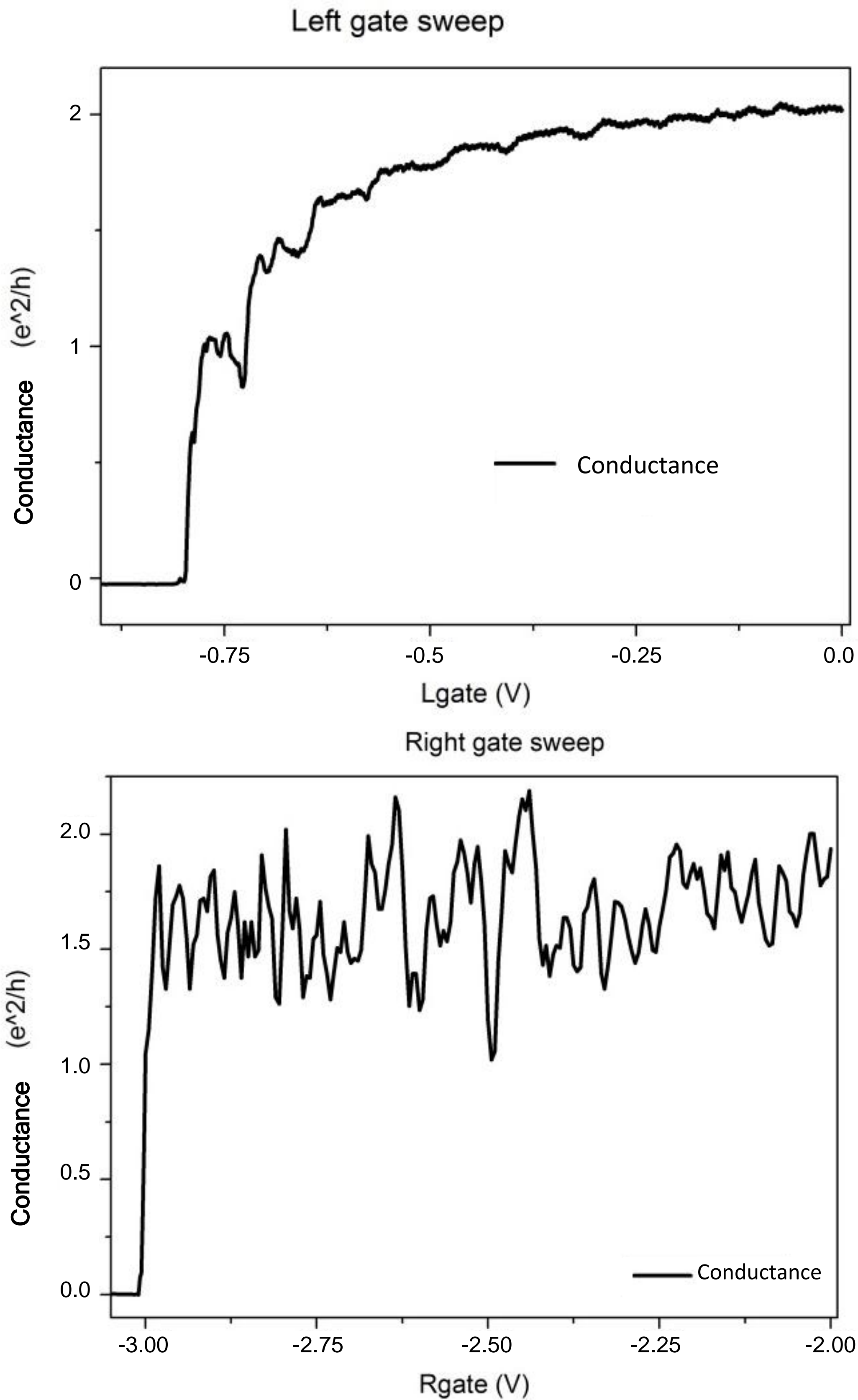

Graph 5.1 – Top-gates sweep. A voltage of 100µV is applied between the channel source and drain. Then, a voltage sweep is carried with one of the gates, while the other is set to 0V, and the current in the channel is measured.

The left gate sweep shows a good gating effect by the top-gate. The current level is almost constant throughout most of the voltage, and then smoothly the current decreases until it reaches no current at around 0.8V. On the other hand, the right top-gate does not show this nice behavior. As it can be seen, there is too much noise in the signal, and after a certain threshold, the current suddenly drops to zero.

Further study on the right gate showed that it has a capacitor-like behavior. If the current was slowly increased to voltages between -2.5 and -3.0V, it could be seen a slight change in current. But as soon as the voltage was higher than -3.0V, the current would start to drop quite fast until the current reaches zero, even if the voltage was not increased anymore. When this gate was set back to zero V again, the current in the channel would remain zero for a long time (order of minutes) until it started to increase, and this increase would be slow. After almost an hour, the original current value would be reached again. The explanation for this effect is probably due to charges that get trapped in the interface between the right top-gate and the HfO_2 film.

It was decided then to avoid sweeping the right gate, since it was unstable. As mentioned in the previous paragraph, the values for the right top-gate were limited to be in between -2.5 to -2.8V, while the left top-gate could be used at any range.

The next step was to measure the magnetic response of the FM gates. Therefore again a voltage was applied between the channel source and drain and the magnetic field was swept a few times.

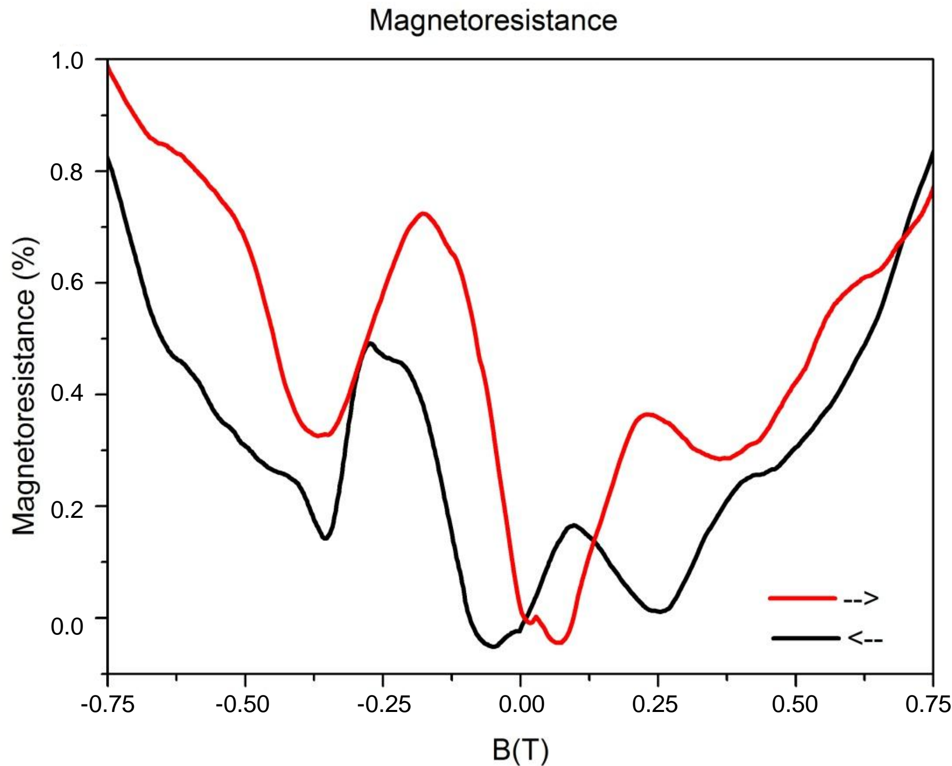

Graph 5.1 – Magnetoresistance versus magnetic field. The red line represents the measured current while the magnetic field was being swept from the negative value to the positive value and the black line represents the magnetic field being swept from the positive to the negative value. Right gate = 0V; left gate = 0V; channel bias = 100µV.

The magnetoresistance (MR) is calculated with the following formula:

$$MR = \frac{(R_0 - R_M)}{R_0} \times 100 \qquad (5.1),$$

where R_0 is the measured resistance at zero magnetic field and R_M is the resistance at the applied magnetic field.

Graph 5.2 shows that there is a change in resistance with a change in the applied magnetic field, but this change is very small, less than 1%. The main valey on both curves are shifted from zero, and as expected due to hysteresis presented in all FM materials. The red line, that represents the field being swept from a negative to a positive value, is shifted to a positive value of the magnetic field (~0.06T), while the black line, which represents the magnetic

field being swept from positive to negative values, is shifted to a negative value (~-0.06T).

Since there is no voltage applied to the top gates, it means that there are a many conducting channels open, allowing scattering, so the polarization of the current is not very efficient.

To decrease the number of conducting channels, a voltage was applied on the top gates so the measured current would be below the value of only one cunducting channel.

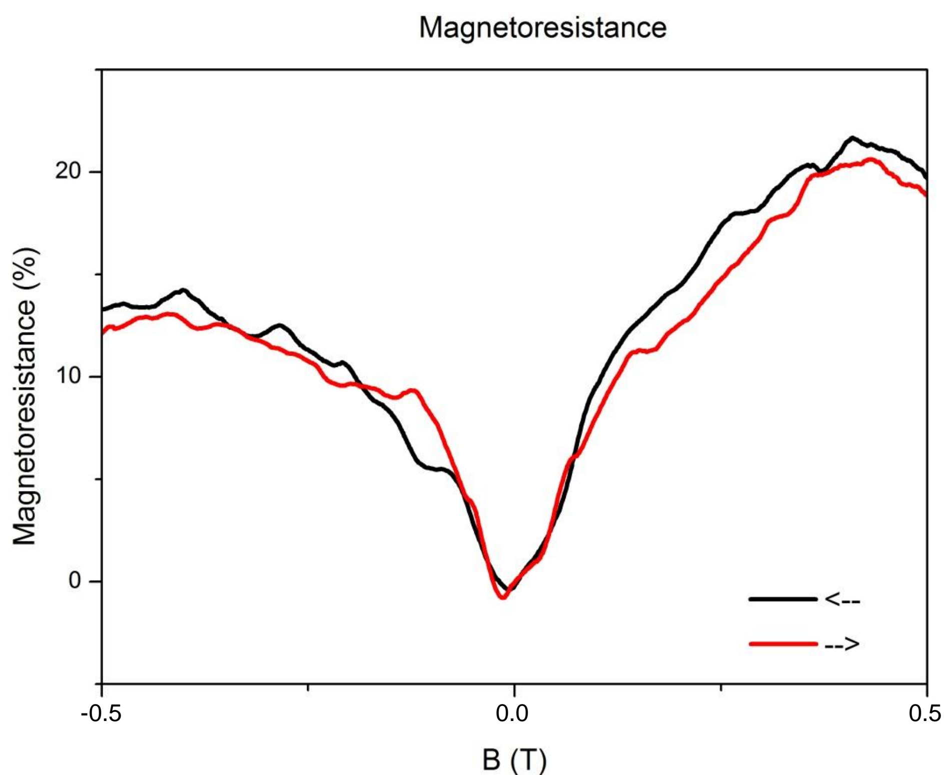

Graph 5.2 – Magnetoresistance versus magnetic field. The red line represents the measured current while the magnetic field was being swept from the negative value to the positive value, and the black line represents the magnetic field being swept from the positive to the negative value. Right gate = -2700mV; left gate = -180mV; channel bias = 100µV.

It can be readily observed that the change in magnetoresistance has increased from less than 1% to approximately 16%, although the hysteresis cannot be seen on this configuration.

Following the same type of measurements, different configurations of the top gates were tried to study the change of the magnetoresistance curve, always having the current levels below one open conducting channel.

To keep things comparable, only one parameter was changed at each new configuration. It was decided to maintain the right channel at -180mV and decrease the right gate to -2500mV, slightly increasing the current values and observe the result.

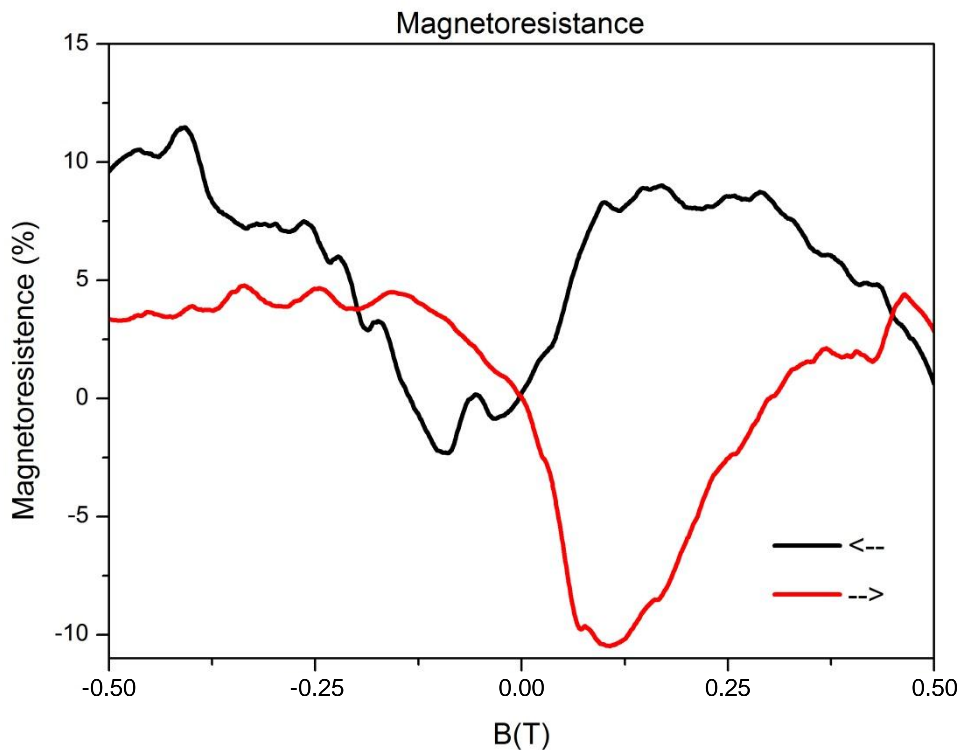

Graph 5.3 - Magnetoresistance versus magnetic field. The red line represents the measured current while the magnetic field was being swept from the negative value to the positive value, and the black line represents the magnetic field being swept from the positive to the negative value. Right gate = -2500mV; left gate = -180mV; channel bias = 100µV.

This graph shows that the magnetoresistance is increased by 15% like the previous one, but this time the hysteresis has been "recovered" at a slightly higher value (~±0.1T). Maintaining the same value for the right gate (-2500mV) and changing the value for the left gate (-150mV), a new measurement was conducted to verify if the hysteresis was still measurable.

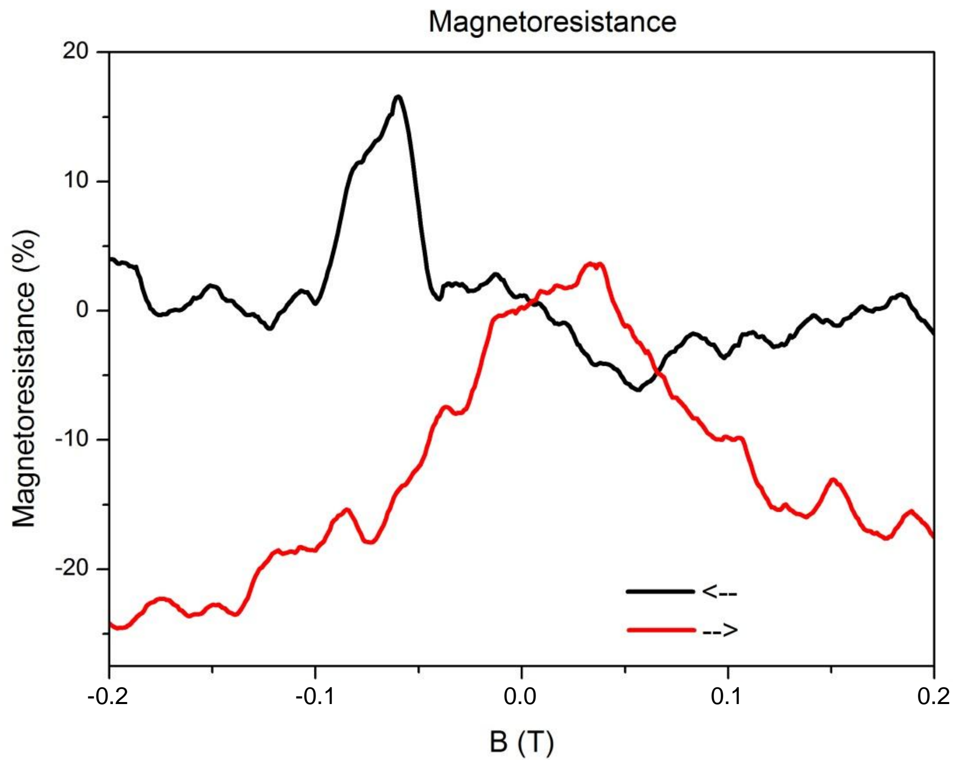

Graph 5.4 - Magnetoresistance versus magnetic field. The red line represents the measured current while the magnetic field was being swept from the negative value to the positive value, and the black line represents the magnetic field being swept from the positive to the negative value. Right gate = -2500mV; left gate = -150mV; channel bias = 100µV.

Again the magnetoresistance increase is around 15%, and the hysteresis around ±0.1T. What is interesting to see is that the shape of the curve has been flipped horizontally, having a more "ʌ" shape, instead of the "v" shape of the previous graphs. To study this effect, it was decided to fix a magnetic field, which was chosen to be 0.6T, keep the right gate at -2500mV and sweep the left gate.

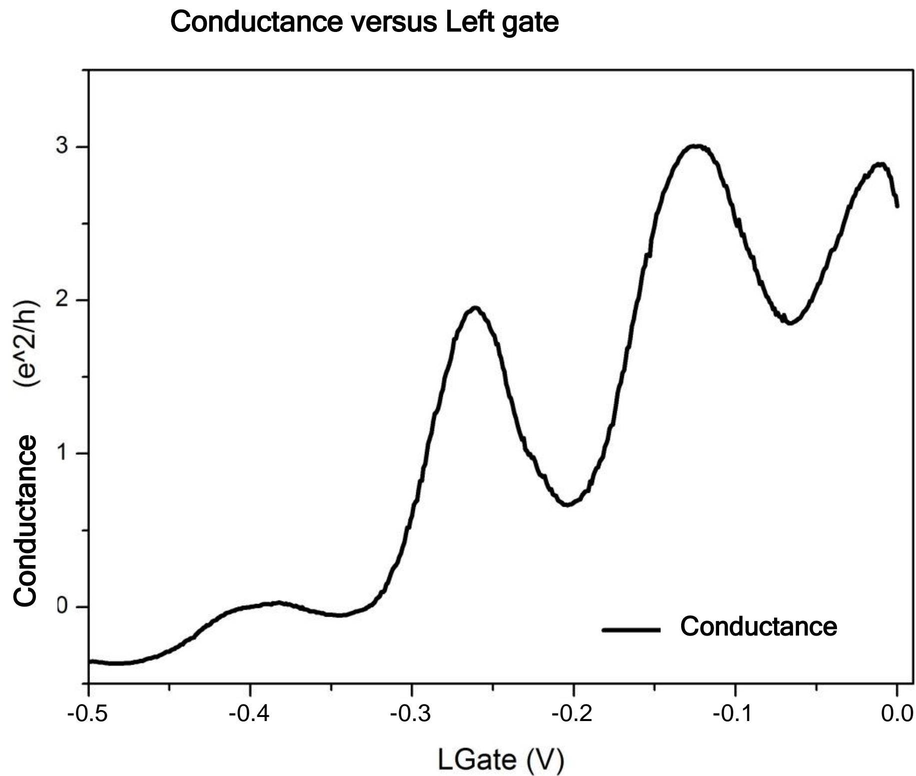

Graph 5.5 – Conductance versus left gate sweep with magnetic field at 0.6T. It can be seen that as the voltage decreases, there are oscillations while the current drops.

For graph 5.2, the value of the left gate is -180mV and on this graph this value falls almost to the very bottom of a valley, while the value of -150mV from graph 5.3 is very close to the top of the peak. To check if this was a coincidence or not, another configuration was chosen with magnetic field at 1T and right gate at -2500mV.

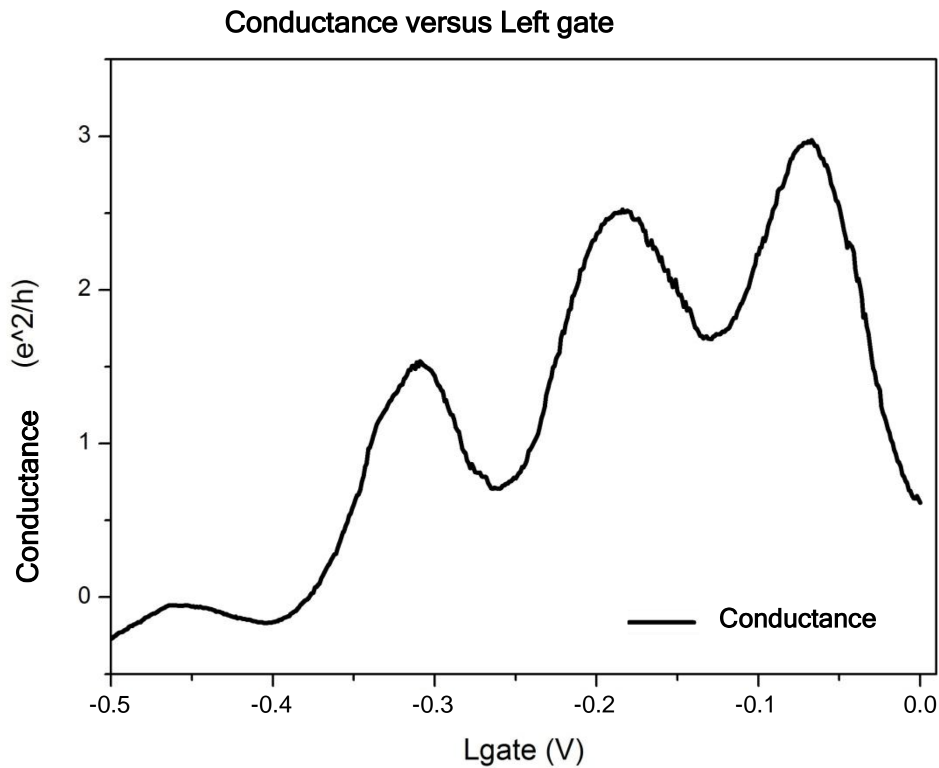

Graph 5.6 – Conductance versus left gate sweep, with magnetic field at 1T. The general behavior of the curve is still the same, but the peaks and valleys are shifted.

Using this result, two values for the left gate were chosen to sweep the magnetic field. The values are -260mV and -200mV, and they are at the valley and at the peak respectively.

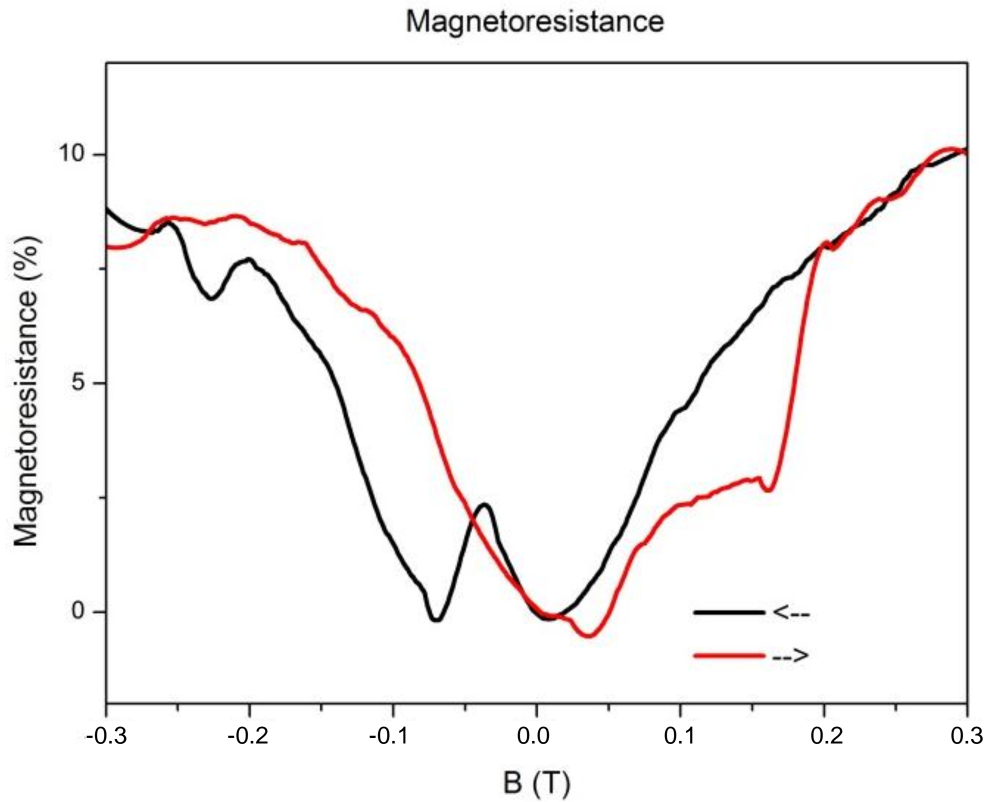

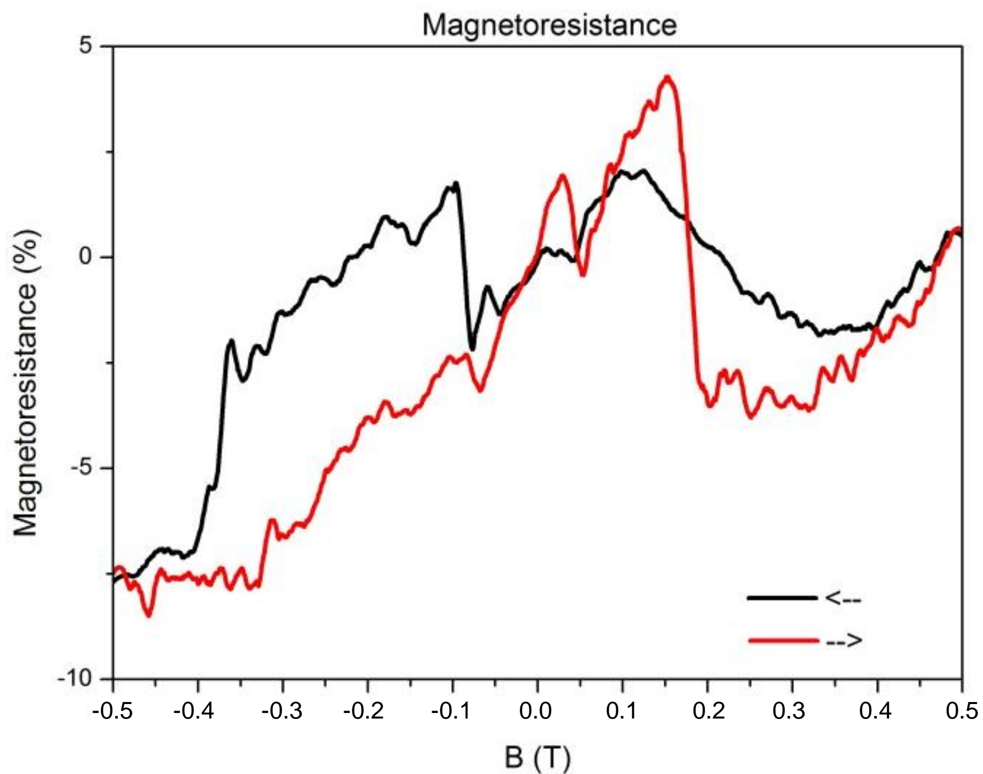

Graph 5.7 - Magnetoresistance versus magnetic field. The red line represents the measured current while the magnetic field was being swept from the negative value to the positive value, and the black line represents the magnetic field being swept from the positive to the negative value. Top) Right gate = -2500mV; left gate = -260mV; channel bias = 100μV; Left) Right gate = -2500mV; left gate = -200mV; channel bias = 100μV.

Once again, there is a difference in overall shape, where the “v” shape comes from the valley of graph 5.7, while the “ʌ” shape comes from the peak. On this configuration, the magnetoresistance change is lower, being a bit less than 10% on both cases.

Because of the leaking problems, charging effects, and lack of time, it was decided that no more measurements would be carried on this sample.

6 Conclusions

It can be concluded that using a nanomagnet to induce polarization and detection of polarized electrons is possible, as the measurements showed both a decrease or increase in resistance up to 16% when the magnetic field is changed and a hysteresis at the curves all around the same value of ±0.1T.

It was also shown that controlling the conductance channels in the 2DEG, the magnetoresistance change was also increased from ~1% to ~16%. This could be explained due to the fact that if only one conductance channel is present and the bands are split due to the Zeeman effect, no band overlap will happen, therefore, a higher percentage of the current in the channel will be polarized. On the other hand, since the right gate (or the detection gate) could not control the conductance the same way, some bands might have been overlapping each other and a poor filtering would result, since both spins, in a different percentage, would be able to pass through that region. Therefore, it is believed that a good right-gate would increase even more the magnetoresistance change.

It was shown that the behavior of the resistance change could be tuned depending on the configuration of the top-gates. Since many of the measurements were difficult to interpret due to charging effects from the right top gate, it was not possible to study this in more details, therefore, it remains in doubt the real possibility of tuning the shape of the curve and its causes.

The Spin-FET could not be done with this design due to fabrication problems. There was a high leakage between the side gates and the channel that made impossible to manipulate the spin precession rate. Again, the charging effects on one of the top gates also made difficult to create and study the equivalent of the spin-valve. Nevertheless, the fabrication and the

substrate can be improved and problems fixed, so this design should be further studied.

7 Outlook

A future work should be able to fabricate a new sample aiming at fixing the following problems. The first should be changing the substrate to the one that PhD student Marcus Larsson uses since the substrate used in this work had a higher doping than the one usually used by him. It was hypothesized by him that higher doping could lead to the leakage, while his devices show no leakage between the side gates and the channel, and both designs have approximately the same channel and etched area dimensions.

The second would be to use Co as a top gate instead of Fe/Co alloy, for the later proved to have a very poor adhesion, while Co is easier to work with and lift-off techniques for this material are well known in the FTF division.

Small changes in the design could also be made to improve the device. Since the orientation of the magnetization used is perpendicular to the soft axes of the nanomagnets, it is hard to reach a saturated state. Therefore there is no abrupt change in the magnetization, but a continuous change takes place instead. The magnetization saturation could be reached, thus the strength of the fringe field increased if the top gates were shifted to the edge of the channel so the soft axes magnetization can be used (figure 7.1).

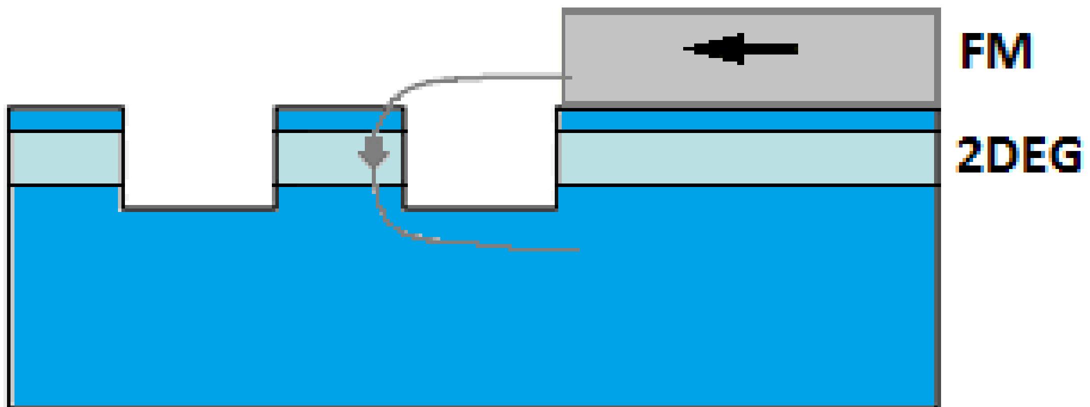

Figure 7.1 – Instead of having the nanomagnet on top of the channel, it can be shifted out of the channel, so the fringe field formed by the magnetization of the soft axes can be used, possibly increasing the field strengh.

8 Acknowledgements

I would like to thank my adviser Prof. Hongqi Xu for both introducing me to this field and giving me the opportunity and the resources to perform this work, not to mention the valuable discussions we had about the work. Also, I would like to thank Marcus Larsson for his help throughout the whole process, ranging from the fabrication processes, measurement techniques and data analysis. My gratitude goes to Waldomiro Paschoal Jr., who besides moral support, provided me with interesting insights into magnetoresistance analysis. I also have to thank the whole nanolab staff for keeping the lab in a good working environment.

9 References

[1] G. E. Moore. (1965). Cramming more components onto integrated circuits. Electronics. 38 (8), 114.

[2] S. E. Thompson, S. Parthasarathy. (2006). Moore's law: the future of Si microelectronics. Materials Today. 9 (6), 20.

[3] M. Radosavljevic, G. Dewey, J. M. Fastenau, J. Kavalieros, R. Kotlyar, B. Chu-Kung, W. K. Liu, D. Lubyshev, M. Metz, K. Millard, N. Mukherjee, L. Pan, R. Pillarisetty, W. Rachmady, U. Shah, and R. Cha. (2010). Non-Planar, Multi-Gate InGaAs Quantum Well Field Effect Transistors with High-K Gate Dielectric and Ultra-Scaled Gate-to-Drain/Gate-to-Source Separation for Low Power Logic Applications. Electron Devices Meeting, 2010 IEE International. 1 (1), 611.

[4] S.A. Wolf, D. D. Awschalom, R.A. Buhrman, J.M. Daughton, S. von Molnar, M. L. Roukes, A. Y. Chtchelkanova, and D. M. Treger. (2001). Spintronics: A spin-based electronics. Vision for the future. Science. 294 (1), p1488-1495.

[5] K. Gilleo, B. Goodrich and G. Nicholls. Available: www.et-trends.com/files/HDD-IMAPS.pdf. Last accessed 14th nov 2011.

[6] S. Datta, B. Das. (1990). Electronic analog of the electro-optic modulator. Applied Physics Letters . 56 (7), 665-667.

[7] A. Rajanikath. (2011). Spin Polarized Feild Effect Transistor (Spin-FET). Available: http://www.nims.go.jp/apfim/SpinFET.html. Last accessed 16th Oct 2011.

[8] Y. Bychkov, E. Rashba. (1984). Oscillatory effects and the magnetic susceptibility of carriers in inversion layers. J. Phys. C: Solid State Phys. 17, p6039-6045.

[9] T. Schäpers . (2007). IBN-1 Quantum and Spin Electronics: Research. Available: http://www2.fz-juelich.de/ibn/index.php?index=377. Last accessed 22nd sep 2011.

[10] Friso Jacobus Jedema. (2002). Theory of spin polarized electron transport. In: Electrical Spin Injection in metallic Mesoscopic Spin Valves. Groningen: RIJKSUNIVERSITEIT GRONINGEN. 11-49.

[11] H.X. Tang, F.G. Monzon, M.L. Roukes, F.J. Jedema, A.T. Filip and B.J. van Wees. (2002). Spin Injection and Transport in Micro- and Nanoscale Devices. In: D. D.Awschalom, N. Samarth and D. Loss Semiconductor Spintronics and Quantum Computation. Berlin: Springer Verlag. 35-51.
[12] S. J. Papadakis, E. P. De Poortere, H. C. Manoharan, M. Shayegan, R. Winkler. (1999). The Effect of Spin Splitting on the Metallic Behavior of a Two-Dimensional System. Science. 28, 2056.
[13] A. T. Filip, B. H. Hoving, F. J. Jedema, and B. J. van Wees . (2000). Experimental search for the electrical spin injection in a semiconductor. Phys. Rev. B. 62 (15), 9996.
[14] I. Žutić, J. Fabian and S. D. Sarma. (2004). Spintronics: Fundamentals and applications. Rev. Mod. Phys.. 76 (2), 323.
[15] I. Turek, V. Drchal, J. Kudrnovský, M. Šob, and P. Weinberger. (1997). Magnetic properties. In: Electronic Structure of Disordered Alloys, Surfaces and Interfaces. Boston: Kluwer. p227.